A multiphase model for the flow of foaming heavy crude oil in a porous medium, with illustrative calculations

P.S. Hammond
9 October 1997

Abstract

This report details work done by the author during a six month secondment from Schlumberger Cambridge Research to Intevep during April to October 1997.

A mathematical description for the flow within a porous permeable medium of oil containing dissolved gas, and capable of liberating that gas when the pressure is dropped to form small bubbles or regions of connected gas, is presented. The intention is that the model will serve as a description for the flow within the reservoir rock of a foamy heavy crude oil. The model consists of a set of conservation or transport equations, together with constitutive functions describing mass transfer processes. Special emphasis is put on investigating the consequences of finite process rates, and non-linearity, in these mass transfer models. The description draws on earlier work of [Joseph], but differs from that in that relative motion between liquid and gas bubbles is allowed, a more elaborate description of exchanges between the phases is used, and variables describing some aspects of the microscale state of the gas bubbles are tracked in time.

The model is used to calculate pressure and volume fraction distributions and time histories in three different, experimentally realisable, situations: slow depressurization of a fluid sample within a sand pack; steady flow through a core under conditions where gas bubbles are evolved and grow during flow within the core; unsteady and non-uniform flow from an initially pressurised and fluid saturated core when the pressure is suddenly dropped at one end.

In the slow depressurization simulations it is found that a mass transfer model based on nucleation theory is capable of reproducing the non-monotonic pressure-time histories observed in experiments, whereas a simpler linear kinetics model is not. In the core flow simulations, again with the nucleation model, a flow rate threshold is found, below which bubble nucleation occurs in a narrow localised zone at pressures close to but a finite amount below the bubble point, and above which nucleation occurs everywhere within the core, continuing at pressures very far below the bubble point. Overall, the size of bubbles is found to increase as the flow rate through the core decreases. It is conjectured that these behaviours may play some part in causing, directly or as a precursor, the experimentally observed dependence of critical gas saturation on flow rate. The approximate core depressurization simulations illustrate some general features of the pressure and volume fraction distributions in this situation, and are of value for checking the results of numerical computations in which all the non-linear terms in the governing equations are present.

Introduction

The aim of this report is to document a mathematical model for the flow within a porous permeable medium of a gas-containing heavy crude oil. The governing transport equations and constitutive laws are set down, and then a series of calculations are performed to demonstrate the capabilities of the model to describe experimentally realisable situations. The work was performed while the author was on a six month secondment to Intevep, from April to October 1997.

Some Venezuelan and Canadian heavy crude oils are termed foamy [Smith], [Loughead & Saltuklaroglu], [Huerta et. al.]. They certainly exhibit obvious foaminess in surface facilities, and it is widely believed that they also behave unusually down hole within the reservoir, at least when pressures there fall sufficiently that dissolved gas is liberated from solution. In Canada, foamy behaviour appears in conjunction with pronounced sand production, and many of the unusual production behaviours there are probably caused by formation failure and creation of high permeability wormholes or channels. Sanding is not considered to be a major factor in Venezuela, and so we shall ignore it and focus on the purely fluid mechanical features of the flow of a gas-containing oil in a porous medium. To avoid confusion, it is probably wise not to mix the Canadian and Venezuelan experiences.

The unusual behaviours exhibited by the so called foaming heavy crudes (FHCs) are usually defined through their contrast with the familiar primary production solution gas drive behaviour experienced with light (i.e. low viscosity) oils [Maini]. When a well penetrating a light crude accumulation is first put on production, the pressure in the formation surrounding the well drops, gas is evolved from solution in the oil, the bubbles occupy a larger volume that the oil from which they were created, and the consequent net volume expansion drives fluid into the well. Initially at least, the gas is present in the form of disconnected bubbles, which are trapped within the pore space of the rock, against the action of viscous and gravitational forces, by capillary forces. It is a matter of experience that this process only produces a few percent of the liquid volume originally in place near the well. Following an initial period of mainly liquid production, large volumes of gas start to flow from the well, and the liquid flow rate drops to a low value. These large gas production rates are interpreted as being the result of the gas bubbles within the formation becoming connected, permitting gas flow over large distances. Once the gas can flow within the formation, pressure gradients in the vicinity of the well fall to low values controlled by the gas viscosity (always less than the liquid viscosity), and this in turn causes the liquid flow rate to drop; the pressure gradient is insufficient to drive a large liquid flow against Darcy resistance. Changing the pressure at which the well is operated does not much affect the total volume of oil recovered. Since oil production is usually more economically attractive than gas production, early gas production is to be avoided, and reservoirs are usually produced by some other process, for example water flooding, which supplies additional energy, beyond that associated with the initial reservoir pressure, to drive the oil from the rock.

By contrast, in the same process of primary recovery by solution gas drive, foamy heavy oil wells are felt to produce a much greater percentage of the original oil in place before massive gas production begins. Figures as high as 25% are quoted [Maini], although 10-15% is probably more usual. This is economically very attractive, since, for example, costly water injection facilities are not necessary to ensure good total volumetric recovery. During the extended phase of predominantly liquid production, the amount of gas flowing from the well is believed to be somewhat lower than would be expected on the basis of the known initial gas content. Additionally, total volumetric recovery is thought to increase with the pressure drawdown applied to the reservoir. While hard field data is not easy to find in the literature, there seems to be broad agreement that the above statements are reasonable, and that there is a difference between this behaviour and that which would be expected of a light oil. The generally accepted interpretation of these observations is that, although the same process of liquid production driven by the volume expansion associated with the creation of bubbles is operating as in the light oil case, other factors operate in foaming heavy oils which permit the liberated bubbles to exist, separate and trapped within the pore space, up to much higher gas volume fractions. Thus, the key difference between foamy and non-

foamy solution gas drive production is the higher value in the former case of the critical gas saturation, which is defined as the volume of the pore space filled with gas at the instant at which flow of gas over large distances becomes possible.

While this interpretation seems reasonable, and would probably be accepted by most workers in the field, there is considerable disagreement over detail, and over the important fluid mechanical processes acting and the controlling material physico-chemical parameters. In conjunction with this lack of agreement over detailed mechanism, there is no agreement on how the formation flow of foamy oils should be modelled mathematically. An additional consequence of this lack of an agreed mechanistic model or explanation is that it is often unclear what is the most illuminating experiment to perform, and also the interpretation of experiments is often controversial. It is hoped that work on mathematical descriptions, such as that proposed here, will help to generate an agreed conceptual framework within which this complex phenomenon can be explored.

The present modelling grows out of work initiated by [Joseph]. His approach, which is presently being extended, and will be the subject of a separate report and publication, is essentially a mixture theory in which the crude oil-gas bubble mixture is treated as a single fluid with effective properties. Now, while such a description is simple, contains parameters which are comparatively easily measured experimentally, and is capable of explaining many of the observed phenomena, it has limitations, particularly in cases where relative motion between the liquid and bubbles are possible and important, or where evolving small scale quantities like the bubble size are of interest. The goal of the present model, which treats the oil and gas as separate flowing phases between which mass transfer can occur, is to permit such situations, outside the scope of the simpler model, to be studied. The model described here is similar to that of [Sheng et. al.], in that it is formulated in similar transport equation plus mass transfer model terms, but we use a more general form of Darcy's law (cross terms are included), allow non-zero capillary pressures, and also carry microscale descriptor variables which permit constitutive functions to be made dependent on details of the gas arrangement on small scales, and implement a more detailed model for mass transfer between the phases. [Sheng et. al.] assume the gas bubbles to move with the liquid, but we allow the velocities to be different. The evolution of the present model can be traced in [Hammond97a] through to [Hammond97e]. It is hoped that this report describes the best presently available form of the model, and corrects earlier errors; the earlier reports contain some results not reported here, but some aspects of the model are not correct (for example the treatment of equilibrium gas solubility). For that reason, it is recommended that future work be based on the equations as stated here.

As well as setting out the framework of a mathematical model for formation flow of foamy crude, solutions are constructed as far as is possible using semi-analytical means, for three different experimentally realisable situations. These situations are: unsteady depressurization of foamy crude within a sand pack, at rates sufficiently low that the pressure and gas volume fraction remain spatially uniform within the pore space of the pack (the so called PVT cell experiment), the principle output of the calculation being a prediction of cell pressure versus time or cell volume; steady but spatially non-uniform flow through a porous permeable core, at fixed volume injection rate and injection pressure above the bubble point (the core flow experiment), the main output of the calculation being the pressure and gas bubble volume fraction distributions as a function of distance from the entrance to the core; unsteady and spatially non-uniform flow within an initially pressurised and foamy crude saturated core, when the pressure on one face of the core is suddenly lowered to a fixed value below the bubble point (the core depressurization experiment), the principle outputs being the time and space varying pressure and gas volume fraction distributions as well as the produced fluid flow rate and composition as a function of time. Because these calculations all refer to situations that can be, or have already been, set up in the laboratory, and because the solutions, at least for the first two, are comparatively easy to construct, they offer a good point of contact between modelling and experiment, and hence an opportunity to make a telling test of the completeness and accuracy of the model. It is strongly recommended that all other models for FHC flow be similarly solved in the same set of situations, and the results compared against experiment, and against each other.

Two observations from the results of the calculations seem significant. In simulations of PVT cell tests, a mass transfer model based on nucleation theory was capable of reproducing the experimentally observed non-monotonic pressure versus time behaviour seen in some experiments, whereas a simpler, linear kinetics model gave rise only to monotonic pressure histories. This is strongly suggestive of the need for non-linear elements in the mass transfer model, if this aspect of experimental behaviour is to be reproduced. In simulations of flow though a core, a threshold flow rate was discovered in simulations mad using the nucleation theory based mass transfer model. Below the threshold flow rate bubble nucleation occurred in a narrow zone, and the average bubble size at cessation of nucleation and non-equilibrium bubble growth increased as the flow rate decreased. Above the threshold flow rate nucleation occurred everywhere within the core, and the bubble size increase very lightly with increasing flow rate. It is conjectured that this transition may in some way be a precursor phenomenon which plays a part in the flow rate sensitivity of critical gas saturation; we might, for example argue that, at fixed total bubble volume fraction, the smaller the bubbles the less likely they are to become connected over large distances. Within the results of the nucleation model, this in turn suggests that critical gas saturation should increase with flow rate, as is indeed observed.

The remainder of this report is arranged as follows: We first define variables and set down the primitive conservation laws for flow of a two component, three phase, mixture within a porous medium. The components are oil and methane, the phases, liquid, continuous gas and dispersed or bubble gas. The primitive transport equations are rearranged into forms that may be more useful in practical calculation. Simplified forms of the basic equations are stated, for a number of special cases; negligible capillary pressure, incompressible flow, flow in which all gas bubbles are trapped. Then, the required constitutive laws are listed, and some suggestions for the forms of the functions which describe mass transfer between dissolved and bubble gas, given. The model is then applied to three situations in turn; PVT cell, core flow, core depressurization. Solutions are computed, and the key features illustrated. The document ends with a brief recapitulation and discussion, during the course of which areas requiring further work are listed.

Transport equations and constitutive laws

There are two flowing components; oil, methane. By component, we mean chemical species, or a group of chemical species which for present practical purposes behave like a single species.

There are three phases; liquid, continuous gas, discontinuous gas or bubbles. Each phase may move under the action of pressure gradients. In principle, any of the components may be present in any of the phases. We shall assume, however, that the oil component is not present in either of the gas phases. The methane component may be present dissolved in oil to together form the liquid phase, or alone may form the continuous gas or bubble phases.

Conservation equations for the masses of liquid, bubble, and continuous gas are

$$\begin{aligned}
\frac{\partial}{\partial t}\left(a S_l \rho_l\right) + \nabla.\mathbf{Q}_l &= -f^{l\to b} - f^{l\to c} \\
\frac{\partial}{\partial t}\left(a S_{gb} \rho_g\right) + \nabla.\mathbf{Q}_{gb} &= f^{l\to b} - f^{b\to c} \\
\frac{\partial}{\partial t}\left(a S_{gc} \rho_g\right) + \nabla.\mathbf{Q}_{gc} &= f^{l\to c} + f^{b\to c}
\end{aligned} \qquad (1)$$

where it is assumed that only the methane component transfers between phases, and transfers from liquid to bubbles ($f^{l\to b}$), liquid to continuous gas ($f^{l\to c}$), and from bubbles to continuous gas ($f^{b\to c}$), are included. The S_i are (pore) volume fractions (saturations) and satisfy

$$S_l + S_{gb} + S_{gc} = 1 \qquad (2)$$

and $0 \le S_i \le 1$. The $\mathbf{Q}_i$ are mass fluxes, and a is the porosity of the porous medium.

The conservation equation for the mass fraction of methane in liquid, x, is

$$\frac{\partial}{\partial t}\left(a S_l r_l x\right) + \nabla.\left(x \mathbf{Q}_l\right) = -f^{l\to b} - f^{l\to c}. \qquad (3)$$

The evolution equation for the local bubble number, N, is

$$\frac{\partial}{\partial t}(a N) + \nabla.\mathbf{q}_{gb}^{N} = n - c^{b\to c} \qquad (4)$$

where n is the number rate of bubble nucleation (per unit volume of porous medium) and $c^{b\to c}$ is the number rate of destruction of bubbles by coalescence into continuous gas. We neglect splitting of the continuous gas, to create new bubbles.

Equations of state for liquid and gas phases are

$$\begin{aligned} \frac{dr_l}{r_l} &= c\,dp - d\,dx \\ \frac{r_g(p)}{r_g(p_{ref})} &= \frac{p}{p_{ref}} \end{aligned} \qquad (5)$$

Constitutive relations for the various mass transfer processes will be considered below. Turning now to the flow rates, we need to link mass and number fluxes to volume fluxes, and volume fluxes to driving forces. The bubble number flux relation is

$$\mathbf{q}_{gb}^{N} = \mathbf{q}_{gb} / V^{av}, \qquad (6)$$

where $\mathbf{q}_{gb}$ is the gas bubble volume flux and V^{av} is the average bubble volume, S_{gb} / N. The bubble mass flux relation is

$$\mathbf{Q}_{gb} = r_{gb}\mathbf{q}_{gb}, \qquad (7)$$

the continuous gas mass flux relation

$$\mathbf{Q}_{gc} = r_{gc}\mathbf{q}_{gc}, \qquad (8)$$

and the liquid mass flux relation

$$\mathbf{Q}_l = r_l \mathbf{q}_l. \qquad (9)$$

In each of these expressions, the density must be evaluated at the appropriate pressure.

For the force-flux relations we use an extended Darcy law in the form

$$\begin{pmatrix} \mathbf{q}_l \\ \mathbf{q}_{gc} \\ \mathbf{q}_{gb} \end{pmatrix} = -\begin{pmatrix} \Lambda_{ll} & \Lambda_{lg} & 0 \\ \Lambda_{gl} & \Lambda_{gg} & 0 \\ \Lambda_{bl} & \Lambda_{bg} & 0 \end{pmatrix}\begin{pmatrix} \nabla p_l \\ \nabla p_{gc} \\ \nabla p_{gb} \end{pmatrix} \qquad (10)$$

where the Λ's are mobilities of the general form $kk_{ij}^{r}(S_{gb}, S_{gc}, N, V^{av}, \ldots)/\mu$, and the ellipses denote other dependencies, for example on the detailed small scale arrangement of the phases (micro-geometry). The form we have chosen for the Darcy laws is like introducing dispersed gas as a third phase in addition to oil and continuous gas, the column of zeros in the mobility matrix ensures that gradients in disconnected gas pressure do not drive any flow. If capillary numbers become large enough, then the Λ's will depend on flow rate too.

Lastly we need to introduce capillary pressure relations

$$\begin{aligned} p_{gc} - p_l &= P_{cap}^{continous}(S_{gc}, \ldots) \\ p_{gb} - p_l &= P_{cap}^{bubble}(V^{av}, \ldots) \end{aligned} \quad , \tag{11}$$

and specify functional forms for the mobilities and capillary pressure as functions of volume fractions, microgeometry, and fluid and rock properties:

$$\begin{aligned} \Lambda_{ll} &= \frac{k}{\mu_l} k_{ll}^{r}(S_l, V^{av}, N, \ldots) \\ \Lambda_{\mathrm{lg}} &= \frac{k}{\mu_l} k_{\mathrm{lg}}^{r}(S_l, S_{gc}, V^{av}, N, \ldots) \\ \Lambda_{gg} &= \frac{k}{\mu_g} k_{gg}^{r}(S_{gc}, \ldots) \\ \Lambda_{gl} &= \frac{k}{\mu_l} k_{gl}^{r}(S_l, S_{gc}, V^{av}, N, \ldots) \\ \Lambda_{bl} &= \frac{k}{\mu_l} k_{bl}^{r}(S_l, V^{av}, N, \ldots) \\ \Lambda_{bg} &= \frac{k}{\mu_l} k_{bg}^{r}(S_l, S_{gc}, V^{av}, N, \ldots) \end{aligned} \tag{12}$$

where k is the single phase permeability of the porous medium and the μ 's are the phase viscosities, together with

$$\begin{aligned} P_{cap}^{continuous} &= \sigma \sqrt{\frac{a}{k}} J(S_{gc}, \ldots) \\ P_{cap}^{bubble} &= 2\sigma / R^{av} \end{aligned} \tag{13}$$

where R^{av} is the average bubble radius, $\left(3V^{av}/4\pi\right)^{1/3}$. The functions k_{ij}^{r} and J are dimensionless. Note that some prejudices about small scale flow physics have been applied, in the choices of the viscosities appearing in the pre-factors of the cross terms, and in the functional dependencies indicated. When the gas bubbles are trapped $\Lambda_{bl} = 0$ and $\Lambda_{bg} = 0$, and when they move with the same velocity as the liquid, $\Lambda_{bl} = \frac{S_{gb}}{S_l}\Lambda_{ll}$ and $\Lambda_{bg} = \frac{S_{gb}}{S_l}\Lambda_{\mathrm{lg}}$.

The initial and boundary conditions that we shall use are

$$\left.\begin{array}{l} p = p^{\infty} \\ S_l = 1 \\ x = x^{\infty} \\ N = 0 \end{array}\right\} \forall \mathbf{x},\ t \le 0 \qquad (14)$$

$$\left.\begin{array}{l} p \to p^{\infty} \\ S_l \to 0 \\ x \to x^{\infty} \\ N \to 0 \end{array}\right\} |\mathbf{x}| \to \infty,\ \forall t \qquad (15)$$

$$p = p^{\infty} - \Delta p, \quad \text{at well, } t > 0. \qquad (16)$$

We assume $p^{\infty} > p^{bubble}$. When the capillary pressure terms are non-zero, we will need to supply a further saturation boundary condition. The produced mass flow rates are

$$\mathbf{Q}_l = -r_l \left(\Lambda_{ll} \nabla p_l + \Lambda_{lg} \nabla p_{gc} \right) \qquad (17)$$

and

$$\mathbf{Q}_g = -r_c \left(\Lambda_{gl} \nabla p_l + \Lambda_{gg} \nabla p_{gc} \right) - r_{gb} \left(\Lambda_{bl} \nabla p_l + \Lambda_{bg} \nabla p_{gc} \right) \qquad (18)$$

per unit area of outflow.

Rearrangements of transport equations

The volume flow rates may be expressed in terms of gradients in the liquid pressure and saturations, using the capillary pressure functions. We have

$$\begin{pmatrix} \mathbf{q}_l \\ \mathbf{q}_{gc} \\ \mathbf{q}_{gb} \end{pmatrix} = -\begin{pmatrix} \left(\Lambda_{ll} + \Lambda_{\mathrm{lg}}\right)\nabla p_l + \Lambda_{\mathrm{lg}} P_{cap}^{gc}{}'\nabla S_{gc} \\ \left(\Lambda_{gl} + \Lambda_{gg}\right)\nabla p_l + \Lambda_{gg} P_{cap}^{gc}{}'\nabla S_{gc} \\ \left(\Lambda_{bl} + \Lambda_{bg}\right)\nabla p_l + \Lambda_{bg} P_{cap}^{gc}{}'\nabla S_{gc} \end{pmatrix}. \tag{19}$$

The main new effect of the cross terms in the Darcy laws on the continuous phase fluxes is to cause saturation gradients, via the capillary pressure term, to have a different effect on the flux of liquid than on the flux of continuous gas. Thus, we expect the cross terms to lead to new phenomena only in situations where capillary pressures are important. For processes in which capillarity is unimportant, cross term effects will also be unimportant, in the sense that there will be no phenomena which could not be predicted on the basis of a theory without cross terms, with appropriate values of the on-diagonal mobilities.

If the each of the three mass conservation equations is divided by the appropriate phase density, the relations linking mass flux to volume flux used, and the results summed, we obtain

$$\begin{aligned} &\sum_{i=l,gb,gc} \left(a S_i \frac{1}{r_i} \frac{\partial r_i}{\partial t} + \frac{1}{r_i} \nabla.\left(r_i \mathbf{q}_i\right) \right) = \\ &\frac{1}{r_l}\left(-f^{l\to b} - f^{l\to c}\right) + \frac{1}{r_{gb}}\left(f^{l\to b} - f^{b\to c}\right) + \frac{1}{r_{gc}}\left(f^{l\to c} + f^{b\to c}\right) \end{aligned}. \tag{20}$$

The time derivatives may be expanded to read

$$\begin{aligned} \sum_{i=l,gb,gc} a S_i \frac{1}{r_i} \frac{\partial r_i}{\partial t} &= \sum_{i=l,gb,gc} a S_i \left(\frac{1}{r_i} \frac{\partial r_i}{\partial p_i} \frac{\partial p_i}{\partial t} + \frac{1}{r_i} \frac{\partial r_i}{\partial x} \frac{\partial x}{\partial t} \right) \\ &= \sum_{i=l,gb,gc} a S_i \left(\frac{1}{r_i} \frac{\partial r_i}{\partial p_i} \left(\frac{\partial p_l}{\partial t} + P_{cap}^{i}{}' \frac{\partial S_i}{\partial t} \right) + \frac{1}{r_i} \frac{\partial r_i}{\partial x} \frac{\partial x}{\partial t} \right) \end{aligned} \tag{21}$$

and the flux divergence to read

$$\sum_{i=l,gb,gc} \frac{1}{r_i} \nabla.\left(r_i \mathbf{q}_i\right) = -\sum_{i=l,gb,gc} \frac{1}{r_i} \nabla.\left(r_i \sum_{j=l,gb,gc} \Lambda_{ij} \left(\nabla p_l + P_{cap}^{j}{}' \nabla S_j \right) \right) \tag{22}$$

where the prime denotes derivative with respect to the appropriate saturation, and several terms in the sums are zero. Combining all these results, we obtain an evolution equation for the liquid pressure

$$\sum_{i=l,gb,gc} a S_i \left(\frac{1}{r_i} \frac{\partial r_i}{\partial p_i} \right) \frac{\partial p_l}{\partial t} - \sum_{i=l,gb,gc} \left(\frac{1}{r_i} \nabla . \left(r_i \sum_{j=l,gb,gc} \Lambda_{ij} \nabla p_l \right) \right)$$
$$= \sum_{i=l,gb,gc} \left(\frac{1}{r_i} \nabla . \left(r_i \sum_{j=l,gb,gc} \Lambda_{ij} P_{cap}^{j} ' \nabla S_j \right) \right) - \sum_{i=l,gb,gc} a S_i \left(\frac{1}{r_i} \frac{\partial r_i}{\partial p_i} P_{cap}^{i} ' \frac{\partial S_i}{\partial t} + \frac{1}{r_i} \frac{\partial r_i}{\partial x} \frac{\partial x}{\partial t} \right) \quad (23)$$
$$+ \left(\frac{1}{r_{gb}} - \frac{1}{r_l} \right) f^{l \to b} + \left(\frac{1}{r_{gc}} - \frac{1}{r_l} \right) f^{l \to c} + \left(\frac{1}{r_{gc}} - \frac{1}{r_{gb}} \right) f^{b \to c}$$

the LHS of which is a diffusion operator, while on the RHS we find a series of saturation and composition change dependent terms, and the by now familiar phase change sources.

Turning now to the liquid saturation, the liquid mass conservation equation may be rewritten as

$$\frac{\partial}{\partial t} \left(a S_l r_l \right) - \nabla . \left(r_l \left(\Lambda_{ll} + \Lambda_{\lg} \right) \nabla p_l \right) = - f^{l \to b} - f^{l \to c} + \nabla . \left(r_l \Lambda_{\lg} P_{cap}^{gc} ' \nabla S_l \right) \quad (24)$$

using the Darcy equations and the capillary pressure relations. But if we sum the expressions for mass flux, and use the capillary pressure relations, we discover

$$\mathbf{Q}_{total} = \sum_{i=l,gb,gc} r_i \mathbf{q}_i = - \left(\sum_{i=l,gb,gc} r_i \sum_{j=l,gb,gc} \Lambda_{ij} \right) \nabla p_l - \sum_{i=l,gb,gc} r_i \sum_{j=l,gb,gc} \Lambda_{ij} \left(P_{cap}^{j} ' \nabla S_j \right) \quad (25)$$

and so

$$\nabla p_l = - \frac{\mathbf{Q}_{total} + \sum_{i=l,gb,gc} r_i \sum_{j=l,gb,gc} \Lambda_{ij} \left(P_{cap}^{j} ' \nabla S_j \right)}{\sum_{i=l,gb,gc} r_i \sum_{j=l,gb,gc} \Lambda_{ij}} \quad (26)$$

whence

$$\frac{\partial}{\partial t} \left(a S_l r_l \right) + \nabla . \left(r_l \frac{\Lambda_{ll} + \Lambda_{\lg}}{\sum_{i=l,gc,gb} r_i \sum_{j=l,gb,gc} \Lambda_{ij}} \mathbf{Q}_{total} \right) = - \left(f^{l \to b} + f^{l \to c} \right)$$
$$+ \nabla . \left(r_l \Lambda_{\lg} P_{cap}^{gc} ' \nabla S_{gc} \right) - \nabla . \left(r_l \frac{\Lambda_{ll} + \Lambda_{\lg}}{\sum_{i=l,gc,gb} r_i \sum_{j=l,gb,gc} \Lambda_{ij}} \sum_{i=l,gc,gb} r_i \sum_{j=l,gb,gc} \Lambda_{ij} P_{cap}^{j} ' \nabla S_j \right) . \quad (27)$$

This form is useful in simple situations where $\mathbf{Q}_{total}$ can sometimes be guessed from the boundary conditions. The equation may be interpreted as follows: the rate of change of the mass of liquid in a given volume element, plus the divergence of the fraction of the total flow that is liquid, equals the mass loss due to evolution of dissolved gas, plus a contribution from flows driven by capillarity (which look like a process of diffusion down saturation gradients).

Considering next the dispersed gas conservation equation, we have

$$\frac{\partial}{\partial t}\left(a\, S_{gb} r_{gb}\right) - \nabla.\left(r_{gb}\left(\Lambda_{bl}+\Lambda_{bg}\right)\nabla p_l\right) = f^{l\to b} - f^{b\to c} + \nabla.\left(r_{gb}\Lambda_{bg} P_{cap}^{gc\,\prime}\nabla S_{gc}\right) \tag{28}$$

or

$$\frac{\partial}{\partial t}\left(a\, S_{gb} r_{gb}\right) + \nabla.\left(r_{gb}\frac{\Lambda_{bl}+\Lambda_{bg}}{\sum_{i=l,gb,gc} r_i \sum_{j=l,gb,gc}\Lambda_{ij}}\mathbf{Q}_{total}\right) = f^{l\to b} - f^{b\to c}$$
$$- \nabla.\left(r_{gb}\left(\Lambda_{bl}+\Lambda_{bg}\right)\frac{\sum_{i=l,gb,gc} r_i \sum_{j=l,gb,gc}\Lambda_{ij}\left(P_{cap}^{j\,\prime}\nabla S_j\right)}{\sum_{i=l,gb,gc} r_i \sum_{j=l,gb,gc}\Lambda_{ij}}\right) + \nabla.\left(r_{bg}\Lambda_{bg} P_{cap}^{gc\,\prime} S_{gc}\right) \tag{29}$$

which is again in fractional flow plus source plus saturation diffusion form. The connected gas saturation follows as $S_{gc} = 1 - S_l - S_{gb}$.

Although these expressions look complicated, they are really no more that the equations familiar in extensions of Buckley-Leverett theory [Hammond91], but with the significant addition of the source terms modelling the consequences of phase change.

The evolution equation for the dissolved gas mass fraction is

$$\frac{\partial}{\partial t}\left(a\, S_l r_l \chi\right) + \nabla.\left(r_l \frac{\Lambda_{ll}+\Lambda_{\mathrm{lg}}}{\sum_{i=l,gc,gb} r_i \sum_{j=l,gb,gc}\Lambda_{ij}}\chi\,\mathbf{Q}_{total}\right) = -\left(f^{l\to b} + f^{l\to c}\right)$$
$$+ \nabla.\left(r_l \chi \Lambda_{\mathrm{lg}} P_{cap}^{gc\,\prime}\nabla S_l\right) - \nabla.\left(r_l \chi \frac{\Lambda_{ll}+\Lambda_{\mathrm{lg}}}{\sum_{i=l,gc,gb} r_i \sum_{j=l,gb,gc}\Lambda_{ij}} \sum_{i=l,gc,gb} r_i \sum_{j=l,gb,gc}\Lambda_{ij} P_{cap}^{j\,\prime}\nabla S_j\right). \tag{30}$$

The evolution equation for the gas bubble number density is

$$\frac{\partial}{\partial t}(a\, N) + \nabla.\left(\frac{N}{S_{gb}}\mathbf{q}_{gb}\right) = n - c^{b\to c} \tag{31}$$

or

$$\frac{\partial}{\partial t}(a\, N) - \nabla.\left(\frac{N}{S_{gb}}\left(\Lambda_{bl}+\Lambda_{bg}\right)\nabla p_l\right) = n - c^{b\to c} + \nabla.\left(\frac{N}{S_{gb}}\Lambda_{bg} P_{cap}^{gc\,\prime}\nabla S_{gc}\right) \tag{32}$$

which may be written

$$\frac{\partial}{\partial t}(a\,N) + \nabla.\left(\frac{N}{S_{gb}} \frac{\Lambda_{bl} + \Lambda_{bg}}{\sum_{i=l,gb,gc} r_i \sum_{j=l,gb,gc} \Lambda_{ij}} \mathbf{Q}_{total} \right) = n - c^{b\to c}$$

$$- \nabla.\left(\frac{N}{S_{gb}} \frac{\left(\Lambda_{bl} + \Lambda_{bg}\right) \sum_{i=l,gb,gc} r_i \sum_{j=l,gb,gc} \Lambda_{ij} \left(P_{cap}^{j} \,'\nabla S_j \right)}{\sum_{i=l,gb,gc} r_i \sum_{j=l,gb,gc} \Lambda_{ij}} \right) + \nabla.\left(\frac{N}{S_{gb}} \Lambda_{bg} P_{cap}^{gc} \,'\nabla S_{gc} \right) \quad . \tag{33}$$

For reference, we note that the total volume flow rate is

$$\mathbf{q}_{total} = \sum_{i=l,gb,gc} \mathbf{q}_i = -\left(\sum_{i=l,gb,gc} \sum_{j=l,gb,gc} \Lambda_{ij} \right) \nabla p_l - \sum_{i=l,gb,gc} \sum_{j=l,gb,gc} \Lambda_{ij} \left(P_{cap}^{j} \,'\nabla S_j \right) \tag{34}$$

and so

$$\nabla p_l = -\frac{\mathbf{q}_{total} + \sum_{i=l,gb,gc} \sum_{j=l,gb,gc} \Lambda_{ij} \left(P_{cap}^{j} \,'\nabla S_j \right)}{\sum_{i=l,gb,gc} \sum_{j=l,gb,gc} \Lambda_{ij}} . \tag{35}$$

In the absence of capillary pressure, we can replace $\mathbf{Q}_{total} \Big/ \sum_{i=l,gb,gc} r_i \sum_{j=l,gb,gc} \Lambda_{ij}$ by $\mathbf{q}_{total} \Big/ \sum_{i=l,gb,gc} \sum_{j=l,gb,gc} \Lambda_{ij}$. The produced mass flow rates are

$$\mathbf{Q}_l = -r_l \left(\left(\Lambda_{ll} + \Lambda_{\mathrm{lg}} \right) \nabla p_l + \Lambda_{\mathrm{lg}} P_{cap}^{gc} \,'\nabla S_{gc} \right) \tag{36}$$

and

$$\mathbf{Q}_g = -r_{gc} \left(\left(\Lambda_{gl} + \Lambda_{gg} \right) \nabla p_l + \Lambda_{gg} P_{cap}^{gc} \,'\nabla S_{gc} \right) - r_{gb} \left(\left(\Lambda_{bl} + \Lambda_{bg} \right) \nabla p_l + \Lambda_{bg} P_{cap}^{gc} \,'\nabla S_{gc} \right) \tag{37}$$

per unit area of outflow.

We remark that the cross terms do not change the structure of the equations compared to the conventional case, but simply change the values of parameters appearing therein, and cause parameters previously equal to become unequal.

Simpler situations

In order to make matters a little clearer, we set down in this section the governing equations in a number of special, simpler, cases.

No capillary pressure

The neglect of the capillary pressure terms simplifies matters a lot (only one pressure, gas density same in continuous and bubble phases, no saturation diffusion terms). Also, in the absence of capillary pressure effects, the presence of cross terms in the Darcy law does not lead to any new phenomena; because the pressures are equal in all phases, flow of, say, oil driven by a gradient in gas pressure cannot be distinguished from flow of oil driven by a gradient of oil pressure. The important equations are:

$$p_l = p_{gb} = p_{gc} \tag{38}$$

$$\mathbf{q}_l = -(\Lambda_{ll} + \Lambda_{\mathrm{lg}})\nabla p_l \tag{39}$$

$$\mathbf{q}_{gc} = -(\Lambda_{gl} + \Lambda_{gg})\nabla p_l \tag{40}$$

$$\mathbf{q}_{gb} = -(\Lambda_{bl} + \Lambda_{bg})\nabla p_l \tag{41}$$

$$\mathbf{Q}_{total} = -\Big(r_l(\Lambda_{ll} + \Lambda_{\mathrm{lg}}) + r_g(\Lambda_{gl} + \Lambda_{gg} + \Lambda_{bl} + \Lambda_{bg})\Big)\nabla p_l \tag{42}$$

$$\begin{aligned}\sum_{i=l,gb,gc} a S_i\left(\frac{1}{r_i}\frac{\partial r_i}{\partial p_i}\right)\frac{\partial p_l}{\partial t} - \sum_{i=l,gb,gc}\left(\frac{1}{r_i}\nabla.\left(r_i \sum_{j=l,gb,gc}\Lambda_{ij}\nabla p_l\right)\right) = \\ -\sum_{i=l,gb,gc} a S_i\left(\frac{1}{r_i}\frac{\partial r_i}{\partial x}\frac{\partial x}{\partial t}\right) + \left(\frac{1}{r_g} - \frac{1}{r_l}\right)(f^{l\to b} + f^{l\to c})\end{aligned} \tag{43}$$

$$\begin{aligned}\frac{\partial}{\partial t}\left(a S_l r_l\right) + \nabla.\left(r_l \frac{\Lambda_{ll} + \Lambda_{\mathrm{lg}}}{r_l(\Lambda_{ll} + \Lambda_{\mathrm{lg}}) + r_g(\Lambda_{gl} + \Lambda_{gg} + \Lambda_{bl} + \Lambda_{bg})}\mathbf{Q}_{total}\right) = \\ -\left(f^{l\to b} + f^{l\to c}\right)\end{aligned} \tag{44}$$

$$\begin{aligned}\frac{\partial}{\partial t}\left(a S_{gb} r_g\right) + \nabla.\left(r_g \frac{\Lambda_{bl} + \Lambda_{bg}}{r_l(\Lambda_{ll} + \Lambda_{\mathrm{lg}}) + r_g(\Lambda_{gl} + \Lambda_{gg} + \Lambda_{bl} + \Lambda_{bg})}\mathbf{Q}_{total}\right) = \\ f^{l\to b} - f^{b\to c}\end{aligned} \tag{45}$$

$$S_{gc} = 1 - S_l - S_{gb} \tag{46}$$

$$\frac{\partial}{\partial t}\left(\phi S_l \rho_l \chi\right) + \nabla.\left(\rho_l \frac{\Lambda_{ll} + \Lambda_{lg}}{\rho_l(\Lambda_{ll} + \Lambda_{lg}) + \rho_g(\Lambda_{gl} + \Lambda_{gg} + \Lambda_{bl} + \Lambda_{bg})} \chi \mathbf{Q}_{total} \right) = -\left(f^{l\to b} + f^{l\to c} \right) \tag{47}$$

$$\frac{\partial}{\partial t}(\phi N) + \nabla.\left(\frac{N}{S_{gb}} \frac{\Lambda_{bl} + \Lambda_{bg}}{\rho_l(\Lambda_{ll} + \Lambda_{lg}) + \rho_g(\Lambda_{gl} + \Lambda_{gg} + \Lambda_{bl} + \Lambda_{bg})} \mathbf{Q}_{total} \right) = n - c^{b\to c} \tag{48}$$

The produced mass flow rates are

$$\mathbf{Q}_l = -\rho_l\left(\left(\Lambda_{ll} + \Lambda_{lg} \right) \nabla p_l \right) \tag{49}$$

and

$$\mathbf{Q}_g = -\rho_g\left(\left(\Lambda_{gl} + \Lambda_{gg} + \Lambda_{bl} + \Lambda_{bg} \right) \nabla p_l \right) \tag{50}$$

per unit area of outflow. The ratio of the produced gas to produced liquid mass flow rates is

$$R = \frac{\rho_g\left(\Lambda_{gl} + \Lambda_{gg} + \Lambda_{bl} + \Lambda_{bg} \right)}{\rho_l\left(\Lambda_{ll} + \Lambda_{lg} \right)}. \tag{51}$$

Gas bubbles move with the liquid, no capillary pressure

In this case, the mobilities Λ_{bl} and Λ_{bg} are related to Λ_{ll} and Λ_{lg}. We have

$$p_l = p_{gb} = p_{gc} \tag{52}$$

$$\mathbf{q}_l = -(\Lambda_{ll} + \Lambda_{lg})\nabla p_l \tag{53}$$

$$\mathbf{q}_{gc} = -(\Lambda_{gl} + \Lambda_{gg})\nabla p_l \tag{54}$$

$$\mathbf{q}_{gb} = -\frac{S_{gb}}{S_l}(\Lambda_{ll} + \Lambda_{lg})\nabla p_l \tag{55}$$

$$\mathbf{Q}_{total} = -\left(\rho_l(\Lambda_{ll} + \Lambda_{lg}) + \rho_g(\Lambda_{gl} + \Lambda_{gg} + \frac{S_{gb}}{S_l}(\Lambda_{ll} + \Lambda_{lg})) \right) \nabla p_l \tag{56}$$

$$\sum_{i=l,gb,gc} \phi S_i \left(\frac{1}{\rho_i} \frac{\partial \rho_i}{\partial p_i} \right) \frac{\partial p_l}{\partial t} - \sum_{i=l,gb,gc} \left(\frac{1}{\rho_i} \nabla.\left(\rho_i \sum_{j=l,gb,gc} \Lambda_{ij} \nabla p_l \right) \right) = - \sum_{i=l,gb,gc} \phi S_i \left(\frac{1}{\rho_i} \frac{\partial \rho_i}{\partial \chi} \frac{\partial \chi}{\partial t} \right) + \left(\frac{1}{\rho_g} - \frac{1}{\rho_l} \right) (f^{l\to b} + f^{l\to c}) \tag{57}$$

$$\frac{\P}{\P t}\left(a\, S_l r_l\right) + \nabla.\left(r_l \frac{\Lambda_{ll} + \Lambda_{\mathrm{lg}}}{r_l(\Lambda_{ll} + \Lambda_{\mathrm{lg}}) + r_g(\Lambda_{gl} + \Lambda_{gg} + \frac{S_{gb}}{S_l}(\Lambda_{ll} + \Lambda_{\mathrm{lg}}))} \mathbf{Q}_{total} \right) = -\left(f^{l\to b} + f^{l\to c} \right) \quad (58)$$

$$\frac{\P}{\P t}\left(a\, S_{gb} r_g\right) + \nabla.\left(r_g \frac{\frac{S_{gb}}{S_l}(\Lambda_{ll} + \Lambda_{\mathrm{lg}})}{r_l(\Lambda_{ll} + \Lambda_{\mathrm{lg}}) + r_g(\Lambda_{gl} + \Lambda_{gg} + \frac{S_{gb}}{S_l}(\Lambda_{ll} + \Lambda_{\mathrm{lg}}))} \mathbf{Q}_{total} \right) = f^{l\to b} - f^{b\to c} \quad (59)$$

$$S_{gc} = 1 - S_l - S_{gb} \quad (60)$$

$$\frac{\P}{\P t}\left(a\, S_l r_l x\right) + \nabla.\left(r_l \frac{\Lambda_{ll} + \Lambda_{\mathrm{lg}}}{r_l(\Lambda_{ll} + \Lambda_{\mathrm{lg}}) + r_g(\Lambda_{gl} + \Lambda_{gg} + \frac{S_{gb}}{S_l}(\Lambda_{bl} + \Lambda_{bg}))} x\, \mathbf{Q}_{total} \right) = -\left(f^{l\to b} + f^{l\to c} \right) \quad (61)$$

$$\frac{\P}{\P t}(a\, N) + \nabla.\left(\frac{N}{S_{gb}} \frac{\frac{S_{gb}}{S_l}(\Lambda_{ll} + \Lambda_{\mathrm{lg}})}{r_l(\Lambda_{ll} + \Lambda_{\mathrm{lg}}) + r_g(\Lambda_{gl} + \Lambda_{gg} + \frac{S_{gb}}{S_l}(\Lambda_{ll} + \Lambda_{\mathrm{lg}}))} \mathbf{Q}_{total} \right) = n - c^{b\to c} \quad (62)$$

The produced mass flow rates are

$$\mathbf{Q}_l = -r_l\left(\left(\Lambda_{ll} + \Lambda_{\mathrm{lg}}\right)\nabla p_l\right) \quad (63)$$

and

$$\mathbf{Q}_g = -r_g\left(\left(\Lambda_{gl} + \Lambda_{gg} + \frac{S_{gb}}{S_l}(\Lambda_{ll} + \Lambda_{\mathrm{lg}})\right)\nabla p_l\right) \quad (64)$$

per unit area of outflow. The ratio of the produced gas to produced liquid mass flow rates is

$$R = \frac{r_g\left(\Lambda_{gl} + \Lambda_{gg} + \frac{S_{gb}}{S_l}(\Lambda_{ll} + \Lambda_{\mathrm{lg}})\right)}{r_l\left(\Lambda_{ll} + \Lambda_{\mathrm{lg}}\right)}. \quad (65)$$

Both fluids incompressible, gas bubbles move with the liquid, no capillary pressure

We assume the liquid density to be constant and independent of composition and pressure. Similarly, the gas density is taken to be constant and pressure independent. We then have

$$p_l = p_{gb} = p_{gc} \tag{66}$$

$$\mathbf{q}_l = -(\Lambda_{ll} + \Lambda_{\mathrm{lg}})\nabla p_l \tag{67}$$

$$\mathbf{q}_{gc} = -(\Lambda_{gl} + \Lambda_{gg})\nabla p_l \tag{68}$$

$$\mathbf{q}_{gb} = -\frac{S_{gb}}{S_l}(\Lambda_{ll} + \Lambda_{\mathrm{lg}})\nabla p_l \tag{69}$$

$$\mathbf{Q}_{total} = -\left(r_l(\Lambda_{ll} + \Lambda_{\mathrm{lg}}) + r_g(\Lambda_{gl} + \Lambda_{gg} + \frac{S_{gb}}{S_l}(\Lambda_{ll} + \Lambda_{\mathrm{lg}}))\right)\nabla p_l \tag{70}$$

$$\mathbf{q}_{total} = -\left(\Lambda_{ll} + \Lambda_{\mathrm{lg}} + \Lambda_{gl} + \Lambda_{gg} + \frac{S_{gb}}{S_l}\left(\Lambda_{ll} + \Lambda_{\mathrm{lg}}\right)\right)\nabla p_l = -\Lambda_{total}\nabla p_l \tag{71}$$

$$\nabla.\left(\left(\Lambda_{ll} + \Lambda_{\mathrm{lg}} + \Lambda_{gl} + \Lambda_{gg} + \frac{S_{gb}}{S_l}\left(\Lambda_{ll} + \Lambda_{\mathrm{lg}}\right)\right)\nabla p_l\right) = \left(\frac{1}{r_g} - \frac{1}{r_l}\right)(f^{l\to b} + f^{l\to c}) \tag{72}$$

$$\frac{\partial}{\partial t}\left(a S_l\right) + \nabla.\left(\frac{\Lambda_{ll} + \Lambda_{\mathrm{lg}}}{r_l(\Lambda_{ll} + \Lambda_{\mathrm{lg}}) + r_g(\Lambda_{gl} + \Lambda_{gg} + \frac{S_{gb}}{S_l}(\Lambda_{ll} + \Lambda_{\mathrm{lg}}))}\mathbf{Q}_{total}\right) = -\left(f^{l\to b} + f^{l\to c}\right)/r_l \tag{73}$$

$$\frac{\partial}{\partial t}\left(a S_{gb}\right) + \nabla.\left(\frac{\frac{S_{gb}}{S_l}(\Lambda_{ll} + \Lambda_{\mathrm{lg}})}{r_l(\Lambda_{ll} + \Lambda_{\mathrm{lg}}) + r_g(\Lambda_{gl} + \Lambda_{gg} + \frac{S_{gb}}{S_l}(\Lambda_{ll} + \Lambda_{\mathrm{lg}}))}\mathbf{Q}_{total}\right) = \left(f^{l\to b} - f^{b\to c}\right)/r_g \tag{74}$$

$$S_{gc} = 1 - S_l - S_{gb} \tag{75}$$

$$\frac{\partial}{\partial t}\left(a S_l \chi\right) + \nabla.\left(\frac{\Lambda_{ll} + \Lambda_{\mathrm{lg}}}{r_l(\Lambda_{ll} + \Lambda_{\mathrm{lg}}) + r_g(\Lambda_{gl} + \Lambda_{gg} + \frac{S_{gb}}{S_l}(\Lambda_{bl} + \Lambda_{bg}))} \chi \mathbf{Q}_{total} \right) = -\left(f^{l\to b} + f^{l\to c}\right)/r_l \tag{76}$$

$$\frac{\partial}{\partial t}(a N) + \nabla.\left(\frac{N}{S_{gb}} \frac{\frac{S_{gb}}{S_l}(\Lambda_{ll} + \Lambda_{\mathrm{lg}})}{r_l(\Lambda_{ll} + \Lambda_{\mathrm{lg}}) + r_g(\Lambda_{gl} + \Lambda_{gg} + \frac{S_{gb}}{S_l}(\Lambda_{ll} + \Lambda_{\mathrm{lg}}))} \mathbf{Q}_{total} \right) = n - c^{b\to c} \tag{77}$$

The produced mass flow rates are

$$\mathbf{Q}_l = -r_l\left(\left(\Lambda_{ll} + \Lambda_{\mathrm{lg}}\right)\nabla p_l\right) \tag{78}$$

and

$$\mathbf{Q}_g = -r_g\left(\left(\Lambda_{gl} + \Lambda_{gg} + \frac{S_{gb}}{S_l}(\Lambda_{ll} + \Lambda_{\mathrm{lg}})\right)\nabla p_l\right) \tag{79}$$

per unit area of outflow. The ratio of the produced gas to produced liquid mass flow rates is

$$R = \frac{r_g\left(\Lambda_{gl} + \Lambda_{gg} + \frac{S_{gb}}{S_l}(\Lambda_{ll} + \Lambda_{\mathrm{lg}})\right)}{r_l\left(\Lambda_{ll} + \Lambda_{\mathrm{lg}}\right)}. \tag{80}$$

Compressible fluids, all gas bubbles trapped, no capillary pressure

Both the mass flux of gas as bubbles, and the number flux of bubbles vanish; $\mathbf{Q}_{gb} = 0$, $\mathbf{q}^N_{gb} = 0$. The associated mobilities Λ_{bl} and Λ_{bg} vanish too. Gas can flow if it becomes connected. The governing equations are now:

$$p_l = p_{gb} = p_{gc} \tag{81}$$

$$\mathbf{q}_l = -(\Lambda_{ll} + \Lambda_{\mathrm{lg}})\nabla p_l \tag{82}$$

$$\mathbf{q}_{gc} = -(\Lambda_{gl} + \Lambda_{gg})\nabla p_l \tag{83}$$

$$\mathbf{q}_{gb} = 0 \tag{84}$$

$$\mathbf{Q}_{total} = -\Big(r_l(\Lambda_{ll} + \Lambda_{lg}) + r_g(\Lambda_{gl} + \Lambda_{gg})\Big)\nabla p_l \tag{85}$$

$$\sum_{i=l,gb,gc} a S_i \left(\frac{1}{r_i}\frac{\partial r_i}{\partial p_i}\right)\frac{\partial p_l}{\partial t} - \sum_{i=l,gb,gc}\left(\frac{1}{r_i}\nabla.\left(r_i \sum_{j=l,gb,gc}\Lambda_{ij}\nabla p_l\right)\right) = -\sum_{i=l,gb,gc} a S_i\left(\frac{1}{r_i}\frac{\partial r_i}{\partial x}\frac{\partial x}{\partial t}\right) + \left(\frac{1}{r_g} - \frac{1}{r_l}\right)\left(f^{l\to b} + f^{l\to c}\right) \tag{86}$$

$$\frac{\partial}{\partial t}\left(a S_l r_l\right) + \nabla.\left(r_l \frac{\Lambda_{ll} + \Lambda_{lg}}{r_l(\Lambda_{ll} + \Lambda_{lg}) + r_g(\Lambda_{gl} + \Lambda_{gg})}\mathbf{Q}_{total}\right) = -\left(f^{l\to b} + f^{l\to c}\right) \tag{87}$$

$$\frac{\partial}{\partial t}\left(a S_{gb} r_g\right) = f^{l\to b} - f^{b\to c} \tag{88}$$

$$S_{gc} = 1 - S_l - S_{gb} \tag{89}$$

$$\frac{\partial}{\partial t}\left(a S_l r_l x\right) + \nabla.\left(r_l \frac{\Lambda_{ll} + \Lambda_{lg}}{r_l(\Lambda_{ll} + \Lambda_{lg}) + r_g(\Lambda_{gl} + \Lambda_{gg})} x\,\mathbf{Q}_{total}\right) = -\left(f^{l\to b} + f^{l\to c}\right) \tag{90}$$

$$\frac{\partial}{\partial t}(a N) = n - c^{b\to c} \tag{91}$$

The produced mass flow rates are

$$\mathbf{Q}_l = -r_l\Big(\big(\Lambda_{ll} + \Lambda_{lg}\big)\nabla p_l\Big) \tag{92}$$

and

$$\mathbf{Q}_g = -r_g\Big(\big(\Lambda_{gl} + \Lambda_{gg}\big)\nabla p_l\Big) \tag{93}$$

per unit area of outflow. The ratio of the produced gas to produced liquid mass flow rates is

$$R = \frac{r_g\big(\Lambda_{gl} + \Lambda_{gg}\big)}{r_l\big(\Lambda_{ll} + \Lambda_{lg}\big)}. \tag{94}$$

We expect this quantity to be one of the most obvious indicators of differences between systems where the gas bubbles are mobile, and systems where they are trapped.

Incompressible flow, all gas bubbles trapped, no capillary pressure

We now consider the phases incompressible, and assume also that the liquid density is independent of composition. The main governing equations become:

$$p_l = p_{gb} = p_{gc} \tag{95}$$

$$\mathbf{q}_l = -(\Lambda_{ll} + \Lambda_{\mathrm{lg}})\nabla p_l \tag{96}$$

$$\mathbf{q}_{gc} = -(\Lambda_{gl} + \Lambda_{gg})\nabla p_l \tag{97}$$

$$\mathbf{q}_{gb} = 0 \tag{98}$$

$$\mathbf{Q}_{total} = -\Big(r_l(\Lambda_{ll} + \Lambda_{\mathrm{lg}}) + r_g(\Lambda_{gl} + \Lambda_{gg})\Big)\nabla p_l \tag{99}$$

$$-\nabla.\Big(\big(\Lambda_{ll} + \Lambda_{\mathrm{lg}} + \Lambda_{gl} + \Lambda_{gg}\big)\nabla p_l\Big) = \left(\frac{1}{r_g} - \frac{1}{r_l}\right)\left(f^{l\to b} + f^{l\to c}\right) \tag{100}$$

$$\frac{\partial}{\partial t}\left(a S_l\right) + \nabla.\left(\frac{\Lambda_{ll} + \Lambda_{\mathrm{lg}}}{r_l(\Lambda_{ll} + \Lambda_{\mathrm{lg}}) + r_g(\Lambda_{gl} + \Lambda_{gg})}\mathbf{Q}_{total}\right) = -\frac{1}{r_l}\left(f^{l\to b} + f^{l\to c}\right) \tag{101}$$

$$\frac{\partial}{\partial t}\left(a S_{gb}\right) = \frac{1}{r_g}\left(f^{l\to b} - f^{b\to c}\right) \tag{102}$$

$$S_{gc} = 1 - S_l - S_{gb} \tag{103}$$

$$\frac{\partial}{\partial t}\left(a S_l \chi\right) + \nabla.\left(\frac{\Lambda_{ll} + \Lambda_{\mathrm{lg}}}{r_l(\Lambda_{ll} + \Lambda_{\mathrm{lg}}) + r_g(\Lambda_{gl} + \Lambda_{gg})}\chi\,\mathbf{Q}_{total}\right) = -\frac{1}{r_l}\left(f^{l\to b} + f^{l\to c}\right) \tag{104}$$

$$\frac{\partial}{\partial t}(a N) = n - c^{b\to c} \tag{105}$$

The produced mass flow rates are

$$\mathbf{Q}_l = -r_l\Big(\big(\Lambda_{ll} + \Lambda_{\mathrm{lg}}\big)\nabla p_l\Big) \tag{106}$$

and

$$\mathbf{Q}_g = -r_g\Big(\big(\Lambda_{gl} + \Lambda_{gg}\big)\nabla p_l\Big) \tag{107}$$

per unit area of outflow. The ratio of the produced gas to produced liquid mass flow rates is

$$R = \frac{r_g\left(\Lambda_{gl} + \Lambda_{gg}\right)}{r_l\left(\Lambda_{ll} + \Lambda_{\mathrm{lg}}\right)}. \tag{108}$$

This set of governing equations represents the simplest situation, and will be studied further in the three special case calculations below.

Constitutive equations for mass transfer terms

In the above formulation, three functions parameterizing mass transfers appear; $f^{l\to b}$ the mass transfer rate from dissolved gas to free gas in the form of bubbles, $f^{l\to c}$ the rate of mass transfer from dissolved gas to free gas in continuously connected form, and $f^{b\to c}$ the mass transfer rate from bubbles to connected gas. We shall consider that mass transfer from dissolved to bubble gas takes place by a combination of two processes, bubble nucleation and subsequent bubble growth. Mass transfer from dissolved gas to continuous gas is assumed to take place by diffusion. Mass transfer from bubble to continuous form is assumed to take place through bubble coalescence (we shall neglect the possibility of splitting of bubbles from masses of continuous gas, and will also neglect splitting of gas bubbles during flow to produce more bubbles of smaller radius). With these ideas in mind, the mass transfer terms may be written in the forms

$$\begin{aligned} f^{l\to b} &= nVr_g + D^{l\to b} \\ f^{l\to c} &= D^{l\to c} \\ f^{b\to c} &= c^{b\to c}V^{av}r_g \end{aligned} \qquad (109)$$

where V is the volume of the new bubbles currently being nucleated, n is the number rate of nucleation of bubbles per unit fluid volume, $c^{b\to c}$ is the number rate of bubble coalescence per unit fluid volume,

$$V^{av} = \frac{S_{gb}}{N} \qquad (110)$$

is the current average bubble volume, and the D terms represent diffusive mass transfers.

Functional forms for the nucleation rate n, the nucleated bubble size V, the various diffusive terms D, and the coalescence rate $c^{b\to c}$ must all be specified in order to close the model. In the two sub-sections below we propose two models for the contributions to $f^{l\to b}$; a simple linear model, and one based on heterogeneous nucleation theory. Here, we shall say nothing about the other two transfer terms, and therefore, for the present, must restrict attention to situations in which they are not important (for example, flows at low gas volume fraction, for which gas bubble coalescence is not an important qualitative contributor to the dynamics).

Before passing to discussion of models for mass transfer, it is worth reviewing the key features of observations from slow depressurization experiments conducted on oil saturated sand packs and cores, since these are the simplest laboratory tests which shed light on transient phenomena during depressurization of a live oil sample. While depressurization of a live oil sample within a PVT cell without any solids present is a still simpler situation, both conceptually and experimentally, the lack of solids undoubtedly means that the process of nucleation of bubbles is different from that occurring when solids are present. For that reason, we focus on observations in the presence of a solid phase. Results showing the time evolution of pressure during a constant volume expansion rate depressurization of an live crude plus porous medium system, held originally at a pressure above the bubble point, have been published by [Huerta et. al.] and [Pooladi-Darvish & Firoozabadi] for heavy oil, and [Firoozabadi, Ottesen & Mikklesen] for light oil.

In all published data, as the cell volume increases, the pressure falls, initially with a large slope corresponding to expansion of a slightly compressible liquid. The pressure falls below the equilibrium bubble point, but the slope of the pressure-volume curve remains liquid-like. At some pressure a finite distance below the equilibrium bubble point, the rate of cell pressure decrease slows, and the pressure

reaches a local minimum and starts to increase. This increase continues for a finite time, until the pressure reaches a level close to, but below the equilibrium bubble point. From that point onwards, the pressure continues to fall, with a small slope characteristic of a gas-liquid mixture. In the paper of [Firoozabadi, Ottesen & Mikklesen] a well characterised light oil system was used, and it was possible to compute with confidence the equilibrium pressure-volume relations. Using these relations, it was found for the light oil that in some cases the pressure-volume behaviour was close to equilibrium, whereas in others, the pressure during the expansion after liberation of gas was always below the expected equilibrium value at the current cell volume.

Two key features emerge from these experiments: First, a finite supersaturation level is required to initiate evolution of gas from solution (that is, the pressure must be dropped a finite amount below the equilibrium bubble point before any gas bubbles are created), and supersaturation may persist, albeit at a reduced level, for long times; second, the rate with which growth of bubbles, and consequent reduction of supersaturation, takes place is finite.

Linear mass transfer law

The simplest possibility is to model the rate of mass transfer from liquid to gas as

$$f^{l\to g} = \begin{cases} \dfrac{S_l r_l (x - Kp_l)}{t} & p_l < p^{bubble} \text{ or } S_{gb} + S_{gc} > 0 \\ 0 & \text{otherwise} \end{cases}, \tag{111}$$

which is a linear relaxation law, driving the dissolved gas mass fraction towards its equilibrium value

$$x^{eq} = Kp_l . \tag{112}$$

The rate of transfer is linearly related to the supersaturation, defined as the difference between the current dissolved gas concentration and that which would obtain at the same pressure but in equilibrium, and we do not distinguish between transfer associated with bubble nucleation or subsequent growth, nor is any account taken of the possibility that a finite supersaturation is required to create the first bubbles and initiate the transfer process. This is probably the simplest possible choice for a constitutive model for mass transfer, depending as it does only on the current values of the state variables, and not their derivatives.

Nucleation and diffusive growth model based mass transfer law

The basis of this model is fully described in [Blander & Katz], and is modified to represent nucleation of bubbles on surfaces, or in surface roughness elements in [Wilt], and is discussed further in [Lubetkin]. We assume that bubbles are nucleated with rate (number of bubbles created per unit time per unit fluid filled volume) given by

$$n = \begin{cases} 0 & x - Kp_l \le 0 \\ C\exp\left(-\dfrac{K^2 B^2 f_2}{(x - Kp_l)^2}\right) & x - Kp_l > 0 \end{cases} \tag{113}$$

and volume

$$V = \frac{4\pi R_{crit}^3}{3} f_1 \tag{114}$$

where

$$R_{crit} = \frac{2\gamma K}{\chi - Kp_l}. \qquad (115)$$

The constant B measures the supersaturation (expressed as a pressure) required to initiate significant nucleation. In classical homogeneous nucleation theory it is related to the gas-liquid interfacial tension and the temperature. The constant C is the maximum rate of bubble creation, and again, for homogeneous nucleation can be related to material properties of the system. Loosely speaking, in the present context it is related to the number of potential nucleation sites, and should increase as the number of such sites increases. The f's are dimensionless shape factors, introduced to represent the consequences of formation of non-spherical bubbles (i.e. bubbles formed in surface roughness elements), and are numerically small. Their net effect is to reduce the supersaturations required for significant nucleation to realistic values, although it must be said that the values of the f parameters are essentially arbitrary (it is well known that for values of B, C given by thermodynamic arguments, the supersaturations required to initiate significant nucleation are, according to this model without the f factors, much larger than are observed in practice). The volume of newly created bubbles is such that they are in (unstable) equilibrium at creation. At low supersaturations, a very small number of large bubbles are nucleated per unit time, while at high supersaturations a large number of small bubbles are created.

The diffusive contribution is modelled as

$$D^{l\to g} = 4\pi R^{av} N D r_l (\chi - Kp_g) f_1 \qquad (116)$$

where

$$R^{av} = \left(\frac{3V^{av}}{4\pi f_1}\right)^{1/3} = \left(\frac{3S_{gb}}{4\pi f_1 N}\right)^{1/3} \qquad (117)$$

and the pressure within the gas bubbles is given by the classical Young-Laplace law,

$$p_g = p_l + \frac{2\gamma}{R^{av}} = p_l + 2\gamma\left(\frac{3S_{gb}}{4\pi f_1 N}\right)^{-1/3}. \qquad (118)$$

Here D is the diffusion coefficient of dissolved gas, and a shape factor appears if the nucleation is heterogeneous and the bubbles are not spheres. The basic idea is that the rate of mass transfer due to diffusion may be estimated as the product of the number of bubbles, the surface area of each bubble, and the diffusivity of dissolved gas times a typical concentration gradient. The concentration gradient is taken to be proportional to the difference between the concentration at the surface of the bubble, and that in the fluid at large distances, divided by the radius of the bubble. The dissolved gas concentration in the liquid close to the bubble surface is assumed to be that which would be in equilibrium with gas at the internal pressure of the bubble, over a flat interface. In all cases, we use the average bubble radius, as estimated from the volume fraction and bubble number density. Within a porous medium we might wish to reduce the value of D, at least when bubbles are approaching the pore size in scale, and also to include some sort of fractal scaling to account for the non-spherical shape of multi-pore clusters [Li & Yortsos], [Satik, Li & Yortsos].

Simulation of PVT cell test

Suppose a sample of FHC is depressurized in a cylindrical cell with a moving piston forming one end. The cross sectional area of the cell is A and the volume is $\mathrm{V}(t)$. The piston moves with speed $U(t)$. If the motion of the piston is sufficiently slow, then all fluid and thermodynamic properties will be spatially uniform within the cell (neglecting hydrostatic pressure differences). If we set $a = 1$, the previous description can be used to compute how fluid properties in the cell change in time, in response to piston motion, and in turn, these results can be used to investigate how cell experiments may be used to estimate some of the constitutive terms appearing in the FHC model.

We begin by deriving a simple result for the time evolution of cell-average fluid properties. The FHC model consists of a set of conservation laws, which may be written

$$\frac{\partial f}{\partial t} + \nabla . \mathbf{j} = s . \tag{119}$$

If we volume integrate this equation over the entire cell, we obtain

$$\frac{d}{dt}\left(\mathrm{V}\,\bar{f}\right) - f\big|_{piston} UA + \mathbf{j}.\mathbf{n}A\big|_{piston} = \mathrm{V}\,\bar{s} \tag{120}$$

where an overbar denotes a cell-averaged value, $\bar{f}\,\mathrm{V} = \int f d\,\mathrm{V}$, $\mathbf{n}$ is the outward unit normal at the piston, and we have assumed that $\mathbf{j}.\mathbf{n} = 0$ on fixed cell walls. Now, the fluxes in the FHC model are all of the form $\mathbf{j} = f\mathbf{q}$ and $\mathbf{q} = U\mathbf{n}$ at the piston. Hence, the piston terms cancel, and we have

$$\frac{d}{dt}\left(\mathrm{V}\,\bar{f}\right) = \mathrm{V}\,\bar{s} . \tag{121}$$

Under the assumption that quantities are uniform throughout the cell, the average of a product is the product of averages, so $\overline{fg} = \bar{f}\bar{g}$, and the average of a function is the function of the average, so $\overline{g(f)} = g(\bar{f})$.

Using these results, and writing the total gas volume fraction as $S_{gb} + S_{gc} = f$, the conservation equations and equations of state give

$$\begin{aligned} \frac{d}{dt}\left((1-\bar{f})\bar{r}_l\,\mathrm{V}\right) &= -\overline{f^{\,l\to g}}\,\mathrm{V} \\ \frac{d}{dt}\left(\bar{f}\,\bar{r}_g\,\mathrm{V}\right) &= \overline{f^{\,l\to g}}\,\mathrm{V} \end{aligned} \tag{122}$$

$$\frac{d}{dt}\left((1-\bar{f})\bar{r}_l\bar{x}\,\mathrm{V}\right) = -\overline{f^{\,l\to g}}\,\mathrm{V} \tag{123}$$

$$\begin{aligned} \bar{r}_l &= \bar{r}_{l0} e^{(c\bar{p} - d\bar{x})} \\ \bar{r}_g &= \frac{r_g(p_{ref})\,\bar{p}}{p_{ref}} \end{aligned} \tag{124}$$

$$\frac{d}{dt}\left(\bar{N}\,\mathrm{V}\right) = \bar{n}\,\mathrm{V} . \tag{125}$$

Suitable initial conditions are

$$\bar{f}(0) = 0 \tag{126}$$

$$\bar{p}(0) = p_0 \tag{127}$$

$$\bar{x}(0) = Kp^{bubble} \tag{128}$$

$$\mathrm{V}(0) = \mathrm{V}_0 \tag{129}$$

$$\bar{N}(0) = 0 \tag{130}$$

with $p_0 > p^{bubble}$. The constant K is the equilibrium solubility; $x^{equilibrium} = Kp$. These equations are completed by specifying either the rate of increase of cell volume, or the rate of change of cell pressure.

Results with linear mass transfer law

For the mass transfer constitutive law we take (111) in the cell averaged form

$$\overline{f^{l\to g}} = \begin{cases} \dfrac{(1-\bar{f})\bar{r}_l(\bar{x} - K\bar{p}_l)}{t} & \bar{p}_l < p^{bubble} \text{ or } \bar{f} > 0 \\ 0 & \text{otherwise} \end{cases} \tag{131}$$

The results of integrating the cell averaged equations with this constitutive law are illustrated in Figures 1 and 3. The first of these illustrates the results of a simulation with constant rate of volume expansion of the cell, the second the results of a simulation with constant rate of pressure decline.

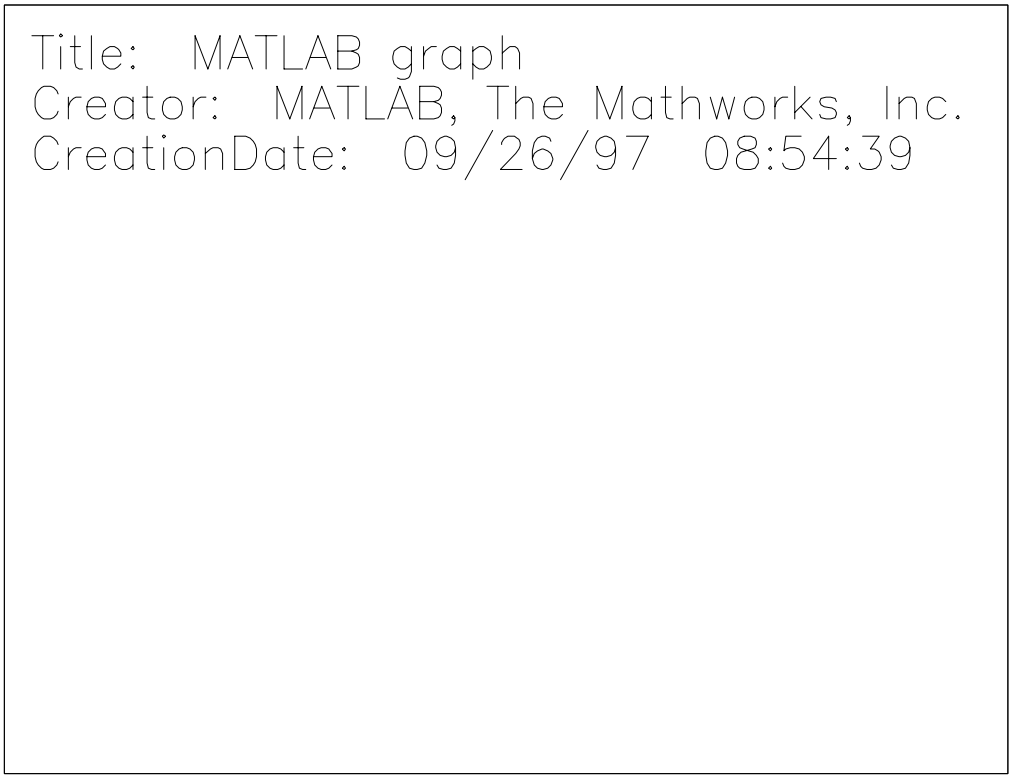

Figure 1: Summary plot of results numerical integration of PVT cell equations, with linear constitutive law, for constant rate increase of cell volume. Solid lines linear constitutive law, dotted lines equilibrium theory. Model parameters: $p^{bubble} = 500$ psi, $K = 1.45*10^{-9}$ Pa^{-1}, $c = 1.45*10^{-9}$ Pa^{-1}, $d = 10^{-1}$, $r_l^{ref} = 1000$ kg m^{-3}, $r_g^{ref} = 100$ kg m^{-3}, $p^{ref} = 1500$ psi, $p^{init} = 1000$ psi, $t = 100$ s, $V(0) = 5*10^{-4}$ m^3, $AU = 5*10^{-7}$ m^3 s^{-1}.

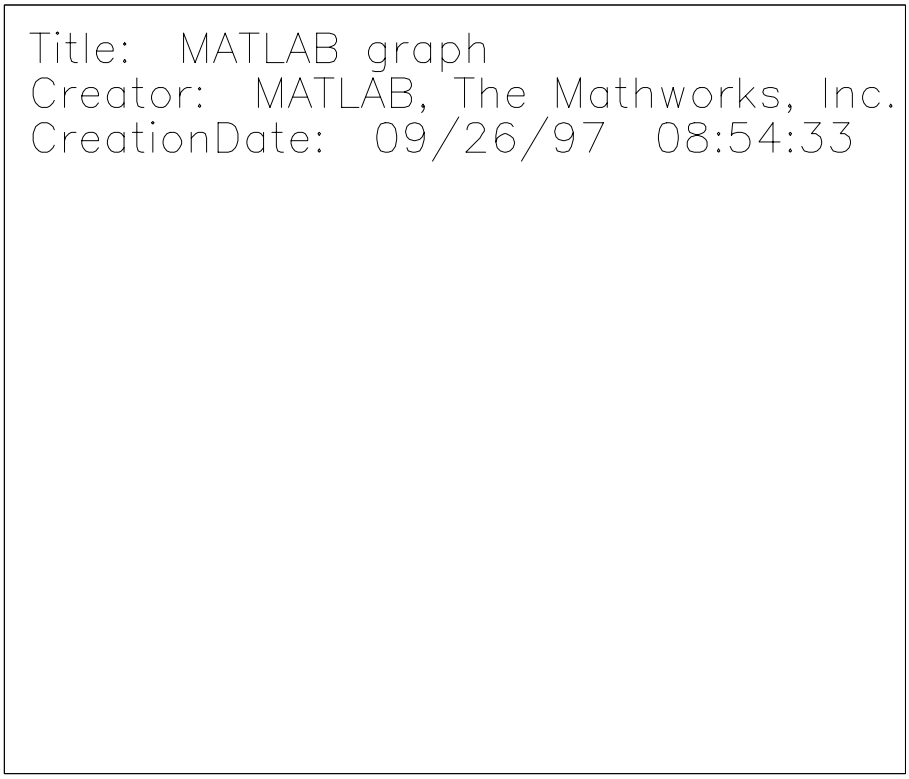

Figure 2: The same, but axes expanded to show details of region near bubble point crossing.

In the constant volume expansion rate simulations we see that as the cell volume increases, the pressure first falls rapidly (corresponding to decompression of a slightly compressible liquid), crosses and falls below the bubble point, and then continues to fall at a much slower rate (corresponding to decompression of a compressible gas-liquid mixture, with effective compressibility enhanced by volume increase due to dissolution of gas). The supersaturation is negative initially, becomes positive once the bubble point is crossed, rapidly reaches a maximum positive value, and then decreases slowly towards zero throughout the rest of the simulation. Pressures are always lower than those corresponding to equilibrium, and there is no sign of a pressure undershoot as is observed in many experimental tests; here, the cell pressure decreases monotonically in time.

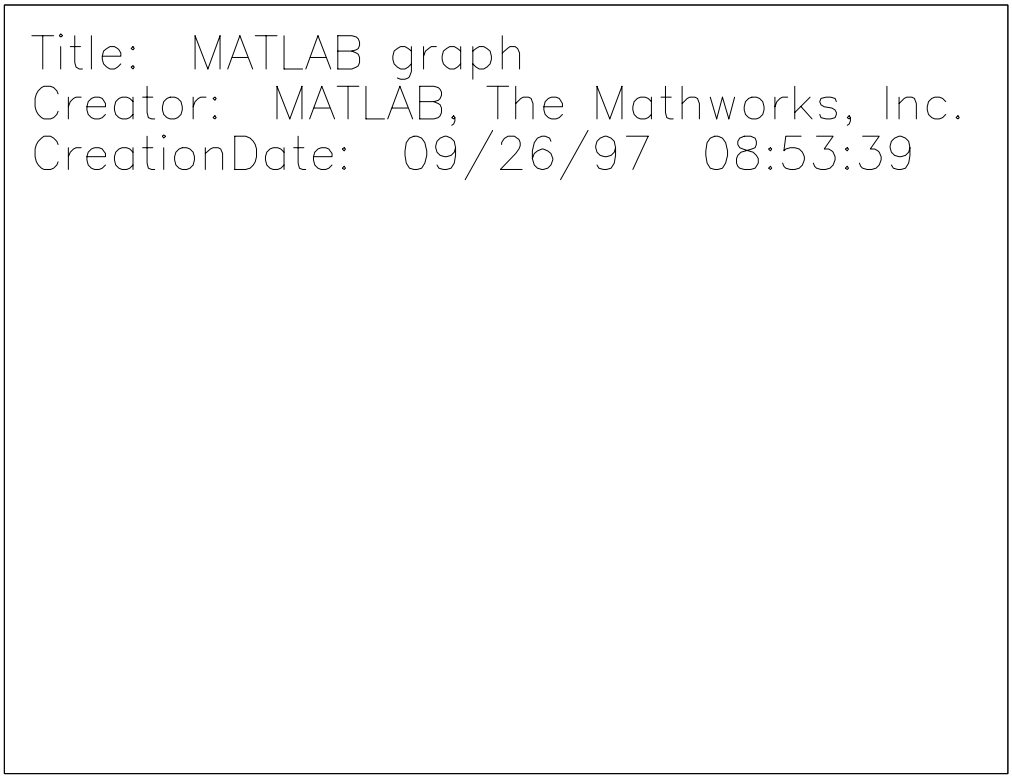

Figure 3: Summary plot of results numerical integration of PVT cell equations, with linear constitutive law, for constant rate of pressure decline. Solid lines linear constitutive law, dotted lines equilibrium theory. Model parameters: $p^{bubble} = 500$ psi, $K = 1.45*10^{-9}$ Pa^{-1}, $c = 1.45*10^{-9}$ Pa^{-1}, $d = 10^{-1}$, $r_l^{ref} = 1000$ kg m^{-3}, $r_g^{ref} = 100$ kg m^{-3}, $p^{ref} = 1500$ psi, $p^{init} = 1000$ psi, $t = 100$ s, $V(0) = 5*10^{-4}$ m^3, $\dot{P} = 6550$ Pa s^{-1} (i.e. about 1 psi s^{-1}).

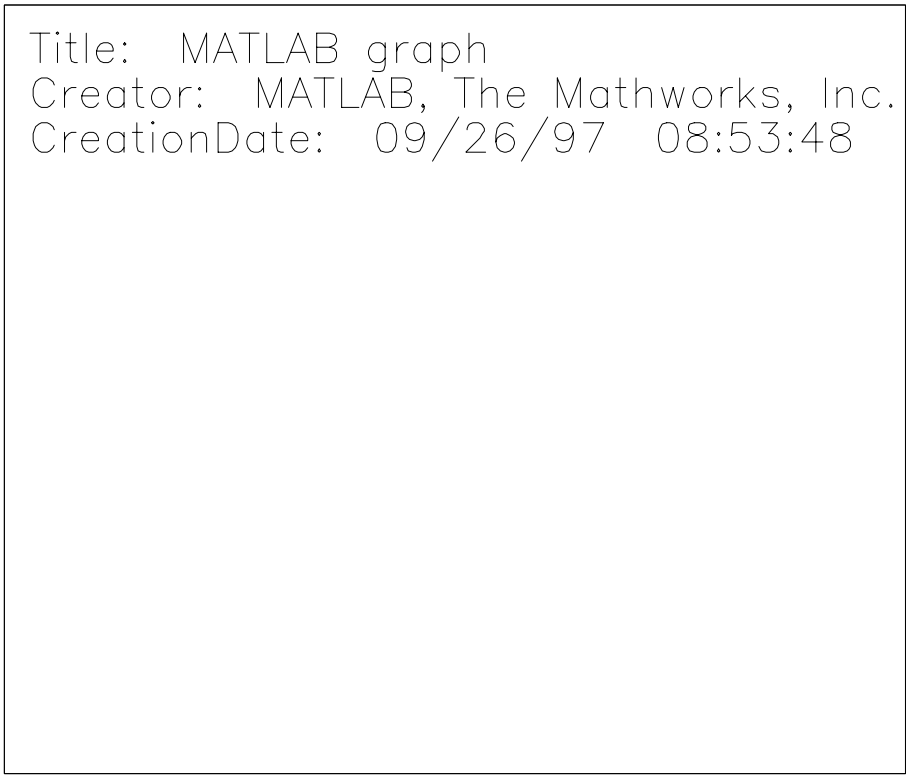

Figure 4: The same, but axes expanded to show details near bubble point crossing.

In the constant pressure decline rate simulations, we again see that the cell pressure is everywhere below that corresponding to equilibrium behaviour, but the supersaturation tends to a finite value at large times (and does not decay to zero as was the case for the constant volume expansion rate simulation). As the pressure falls, or the cell volume increases, the gas volume fraction increases and with it the effective compressibility of the mixture. In order to maintain a constant rate of pressure decline, the rate of volume expansion must thus increase with time, and so the mass transfer relaxation rate becomes ever longer compared with the time scale for cell volume increase. The consequence is that supersaturation levels must stay high in order to drive mass transfer at a finite rate from liquid to gas.

Results with nucleation model

We take the mass transfer to be given by

$$\overline{f^{l\to g}} = n(\bar{f}, \bar{N}, \bar{p}_l, \bar{x})\frac{\bar{f}}{\bar{N}}\bar{r}_g(\bar{p}) + D^{l\to g}(\bar{f}, \bar{N}, \bar{p}_g, \bar{x}) \qquad (132)$$

where the functions n and $D^{l\to g}$ are given by (113) and (116). The results of integrating the cell averaged equations are shown in Figures 5 and 7. Again, the first pair of plots show results of a simulation run in constant volume expansion rate mode, the second pair, a simulation run in constant pressure decline rate mode.

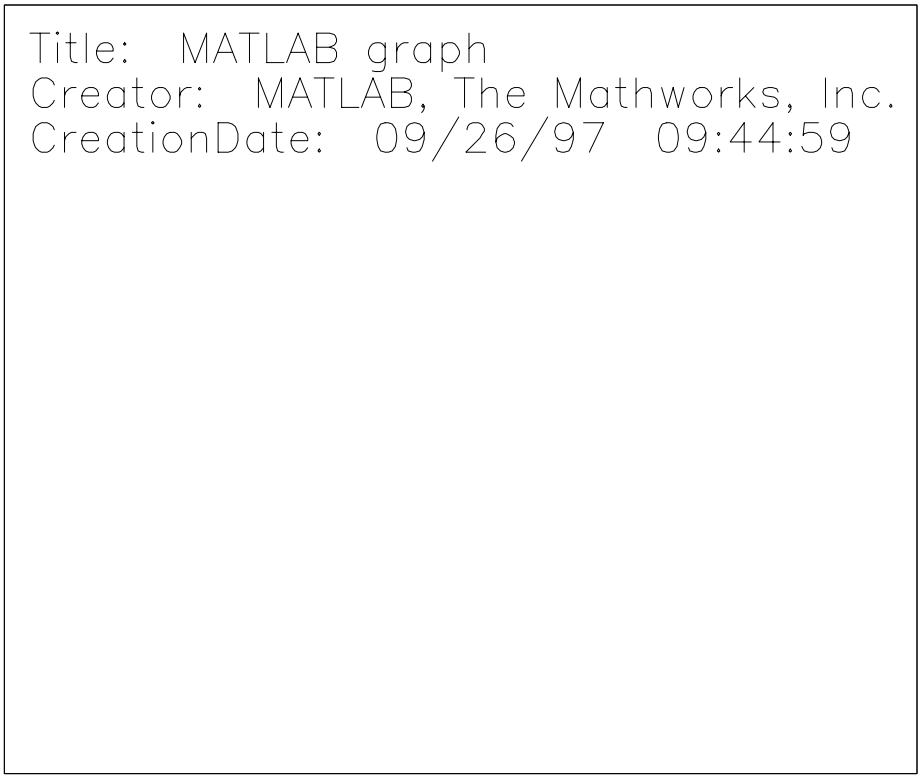

Figure 5: Summary plot of results numerical integration of PVT cell equations with mass transfer given by nucleation model, for constant rate of increase of cell volume. Solid lines nucleation model, dotted lines equilibrium theory. Model parameters: $p^{bubble} = 500$ psi, $K = 1.45*10^{-9}$ Pa^{-1}, $B = 10^{5}$ Pa, $C = 10^{10}$ m^{-3} s^{-1}, $D = 10^{-9}$ m^{2} s^{-1}, $\gamma = 0.02$ Nm, $c = 1.45*10^{-9}$ Pa^{-1}, $d = 10^{-1}$, $r_l^{ref} = 1000$ kg m^{-3}, $r_g^{ref} = 100$ kg m^{-3}, $p^{ref} = 1500$ psi, $p^{init} = 1000$ psi, $V(0) = 5*10^{-4}$ m^{3}, $AU = 5.556*10^{-7}$ m^{3} s^{-1}, $f_1 = f_2 = 0.1$.

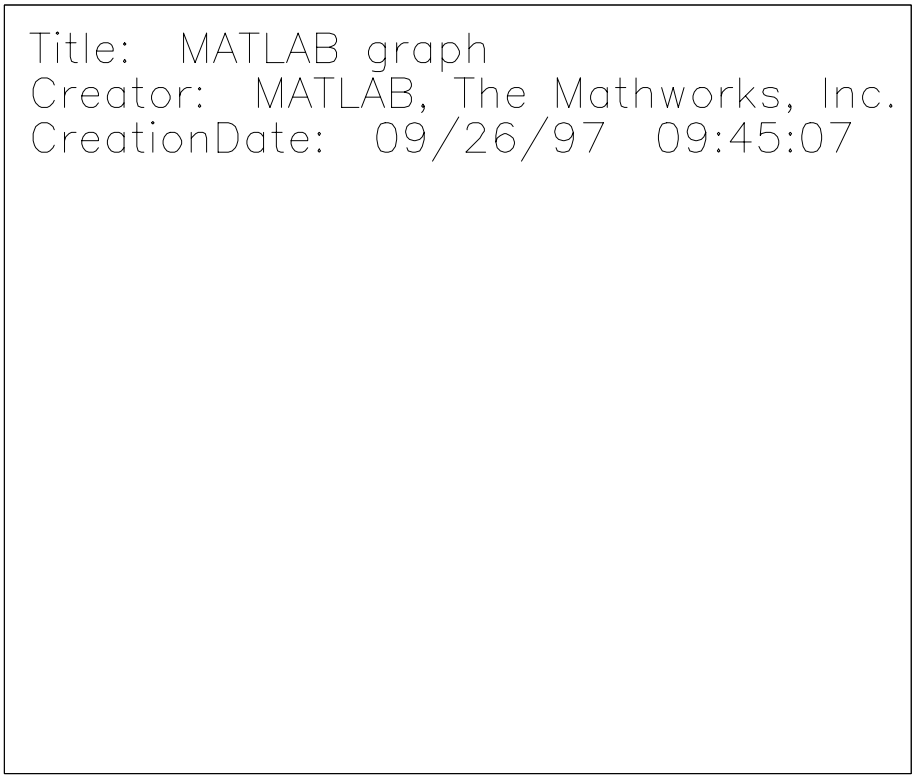

Figure 6: The same, enlargement of region near bubble point crossing.

Examining first the pressure-volume behaviour, we see as before regions of initial rapid pressure decline, corresponding to decompression of liquid, and late slow pressure decline, corresponding to decompression of a gas-liquid mixture with gas dissolution. Between these regions however, the pressure is non-monotonic in time; there is an undershoot, followed by an increase up to (below) the equilibrium pressure-volume line. Similar results have been computed by [Firoozabadi & Kaschiev], and of course, are seen in many experiments. Since this behaviour is not exhibited by the linear mass transfer model, we can conclude that is it a consequence of the non-linearity introduced with the nucleation model, in particular, the finite supersaturation required to initiate bubble nucleation and mass transfer.

A qualitative explanation of the undershoot is straightforward: As the cell expands, pressure falls below the bubble point, and initially, no bubbles are present. The pressure continues to fall at a liquid compressibility determined rate, and eventually the bubble nucleation rate becomes finite once a sufficiently large supersaturation level is created. Bubbles then begin to appear, but the rate of mass transfer into these bubbles is initially not large; it increases as the bubble size, number, and total surface area increase, and eventually becomes significant. Because the rate of mass transfer and consequent creation of bubble volume is initially not large (either because the volume of nucleated bubbles is small, or the diffusion rate into bubbles is small), the cell pressure continues to fall. Eventually however, enough bubbles are present that the rate of diffusive mass transfer becomes significant. Gas then moves rapidly from solution into bubbles, and the associated increase in mass of free gas causes the cell pressure to increase (essentially because processes which would cause an increase in total fluid volume, were free expansion possible, are taking place). The increase in pressure, and decrease in dissolved gas concentration lead to a decrease in supersaturation and a decrease in bubble nucleation rate. At the same time, the effective compressibility of the mixture in the cell increases, and so the subsequent rate of pressure decline decreases. From this point on, the system behaves similarly to the predictions of the linear model, or indeed of equilibrium theory.

The above comments about nucleation rates are borne out in the plots of N versus cell volume or supersaturation. Most of the bubbles are created during the pressure undershoot phase. Note that N decreases at large times because it is defined as the number of bubbles per unit volume, and while the total number of bubbles is constant, the cell volume is increasing.

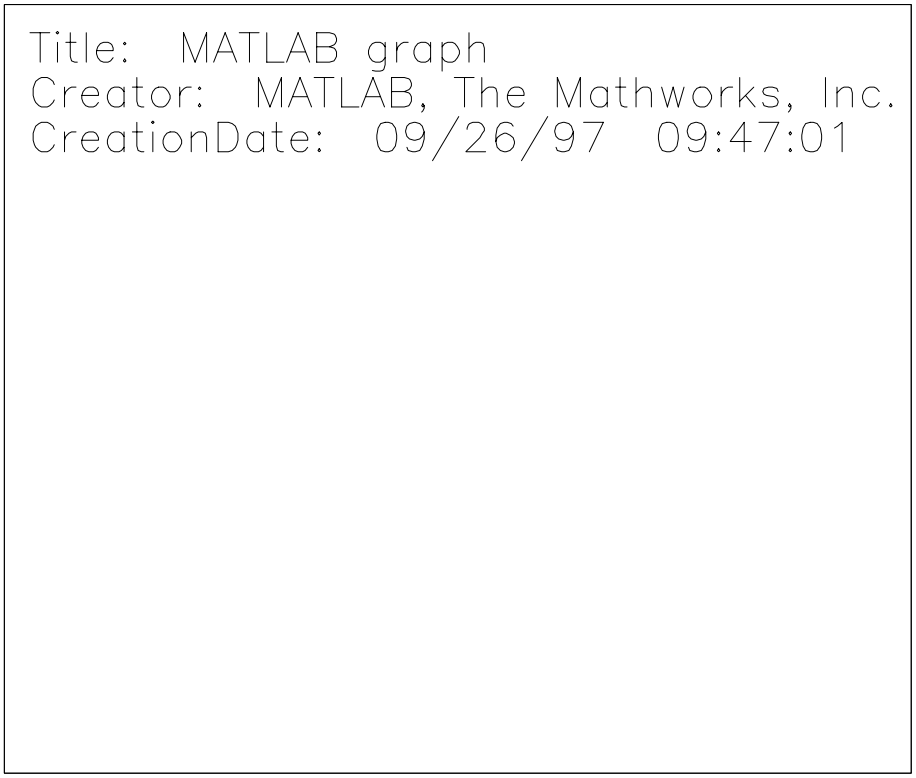

Figure 7: Summary plot of results numerical integration of PVT cell equations with mass transfer given by nucleation model, for constant rate of pressure decrease. Solid lines nucleation model, dotted lines equilibrium theory. Model parameters: $p^{bubble} = 500$ psi, $K = 1.45*10^{-9}$ Pa^{-1}, $B = 10^5$ Pa, $C = 10^{10}$ m^{-3} s^{-1}, $D = 10^{-9}$ m^2 s^{-1}, $\gamma = 0.02$ Nm, $c = 1.45*10^{-9}$ Pa^{-1}, $d = 10^{-1}$, $r_l^{ref} = 1000$ kg m^{-3}, $r_g^{ref} = 100$ kg m^{-3}, $p^{ref} = 1500$ psi, $p^{init} = 1000$ psi, $V(0) = 5*10^{-4}$ m^3, $\dot{P} = 6895$ Pa s^{-1} (approximately 1psi s^{-1}), $f_1 = f_2 = 0.1$.

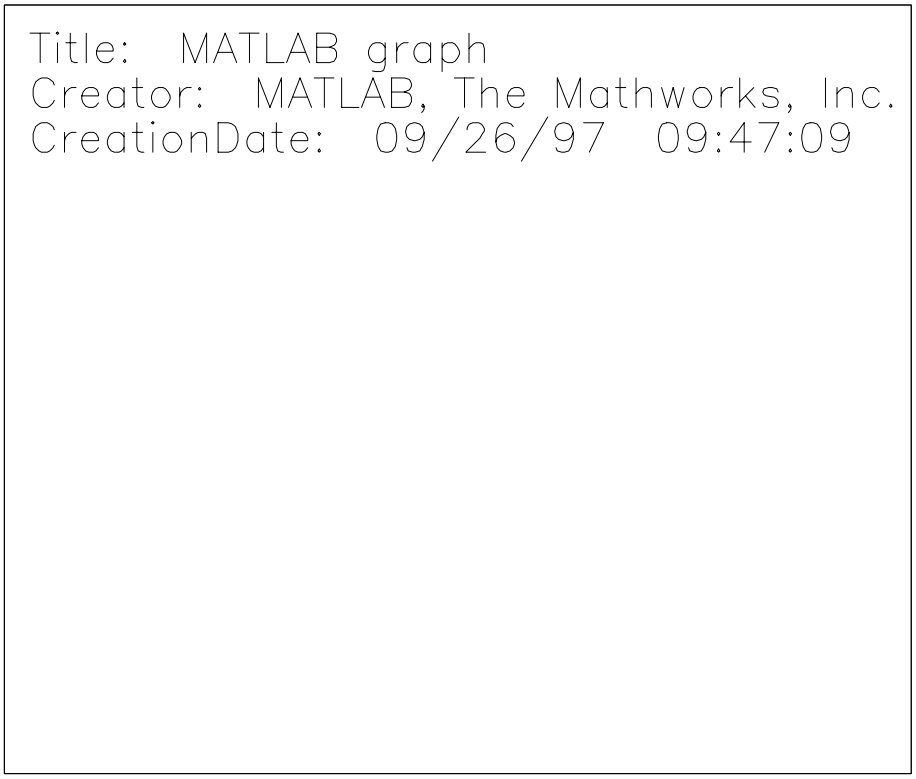

Figure 8: The same, region near bubble point crossing enlarged.

In the constant pressure decline rate simulations, we see rather similar pressure-volume response in the present model to that generated by the linear mass transfer law. Again, at large times a finite supersaturation level appears to be maintained, in contrast to the supersaturation decay seen in the constant volume expansion rate simulation. Clearly, there is no pressure undershoot in this situation.

Simulations of constant pressure decline rate PVT cell tests not reported here show that the total number of bubbles created is an increasing function of the rate of pressure decline.

Further information on the behaviour of bubble nucleation and growth models, including a discussion of the importance of viscous effects, and of means to model the consequences of a bubble size distribution, can be found in [Barclay et. al.], [Toramaru89] and [Toramaru95].

Simulation of steady incompressible flow through a core

We now study a situation that is non-uniform in space, but steady in time. Consider one dimensional flow through a cylindrical porous permeable core of length L and cross sectional area A. Gas saturated liquid enters through the face of the core at $x = 0$, the total injection volume flow rate is Aq_0, and the injection pressure is $p = p^{bubble}$. Fluid leaves the core at $x = L$. We assume that all the gas bubbles, which are liberated as the fluid decompresses within the core, move with the liquid, that both liquid and gas are incompressible and that the liquid density is independent of the mass fraction of dissolved gas, and that the flow is steady. Experimental results in this situation are published by [Maini & Sarma], although unfortunately they do not give data on volume fraction distribution (for which imaging technology is required).

Rearranging the basic transport equations we find

$$\frac{dS_{gb}}{dx} = \frac{\dfrac{1-S_{gb}}{r_l} + \dfrac{S_{gb}}{r_g}}{q} f^{l\to b} \tag{133}$$

$$\frac{dp}{dx} = -\frac{q}{\Lambda} \tag{134}$$

$$\frac{dq}{dx} = \left(\frac{1}{r_g} - \frac{1}{r_l}\right) f^{l\to b} \tag{135}$$

$$\frac{dx}{dx} = -\left(\frac{1-x}{S_l}\right)\frac{f^{l\to b}}{r_l q} \tag{136}$$

$$\frac{dN}{dx} = \frac{n - N\left(\dfrac{1}{r_g} - \dfrac{1}{r_l}\right) f^{l\to b}}{q} \tag{137}$$

subject to

$$S_{gb}(0) = 0 \tag{138}$$

$$p(0) = p^{bubble} \tag{139}$$

$$x(0) = Kp^{bubble} \tag{140}$$

$$q(0) = q_0 \tag{141}$$

$$N(0) = 0. \tag{142}$$

This system can easily be integrated forward from $x = 0$ numerically, once forms for the transfer terms are given. The length of the core should be chosen so that the pressure does not fall below zero within the core.

Results with linear mass transfer law

Using the linear mass transfer law, we obtain the results illustrated in Figures 9 and 10. The total inlet flow rate to the core is the same in both Figures but the first of these has a relaxation rate which is 10 times longer than the second. The outlet flow rate, and gas volume fraction at exit, are slightly greater with the smaller relaxation rate. In both cases we see that the bubble volume fraction, flow rate, and supersaturation increase with distance into the core, but the distance required for the supersaturation to grow to its fully developed value, or for bubble volume fraction to attain a linear rate of growth with distance, is greater for the long relaxation time than for the short. In addition, the limiting value of supersaturation is 10 times larger for the longer relaxation time case. In both cases, the pressure falls linearly with distance, the additional flow rate associated with the volume increase due to creation of bubbles being small.

The different limiting supersaturation values in the two cases can be understood as follows: As a packet of fluid moves through the core it experiences a falling pressure, which causes gas to be evolved from solution. In both cases illustrated here, because the volume flow rates through the core are roughly the same, the Lagrangian rates of pressure decrease are also roughly the same, and hence, the rates of gas evolution must be the same. Since in the linear mass transfer model the rate of gas evolution depends on the supersaturation divided by the time constant, in order for the rates to be equal, the supersaturations must differ by a factor of 10 if the time constants differ by this amount.

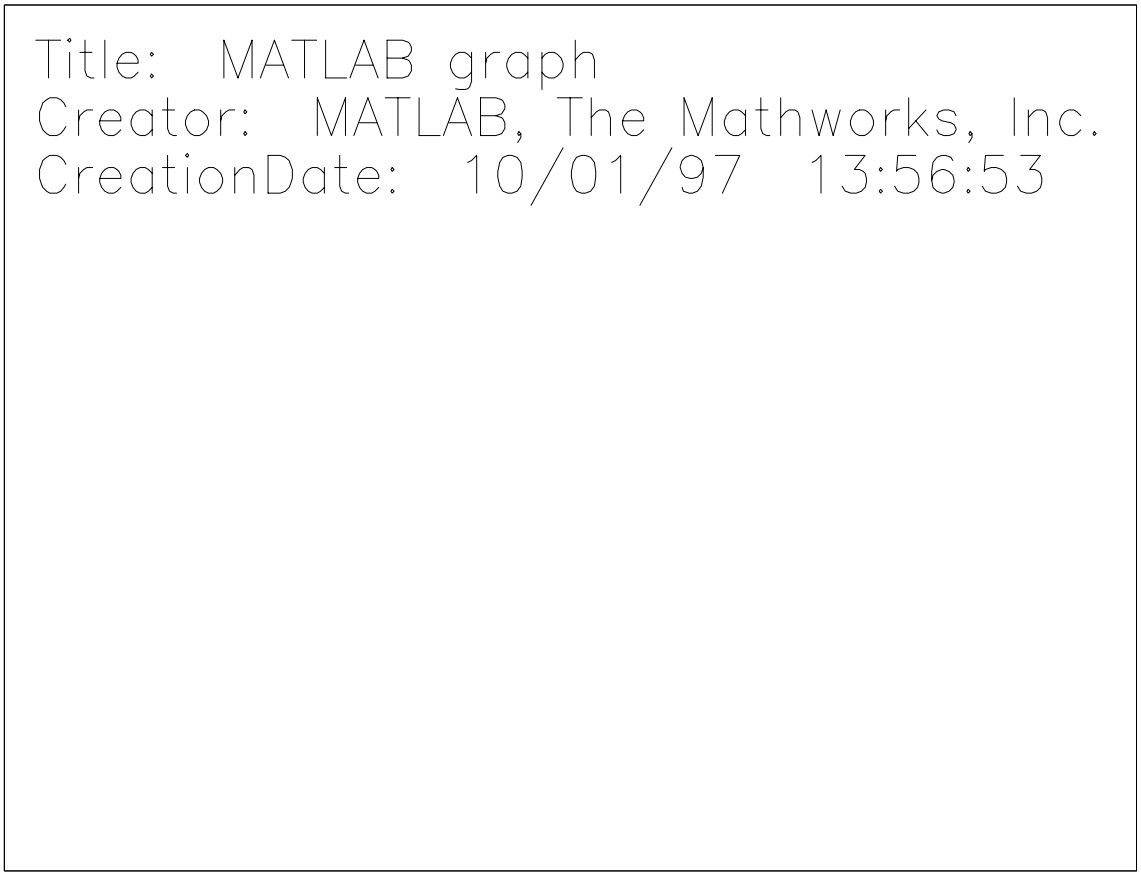

Figure 9: Summary of results of integration of steady core flow equations, with linear mass transfer model. Slow relaxation, $t = 1000$ s. Inlet flow rate $q_0 = 10^{-5}$ ms^{-1}. Other parameters $p^{bubble} = 500$ psi, $K = 1.45 * 10^{-9}$ Pa^{-1}, $r_l^{ref} = 1000$ kg m^{-3}, $r_g^{ref} = 100$ kg m^{-3}, $p^{ref} = 1500$ psi, $\Lambda = 10^{-12}$ m^2 /Pa.s, $a = 0.3$.

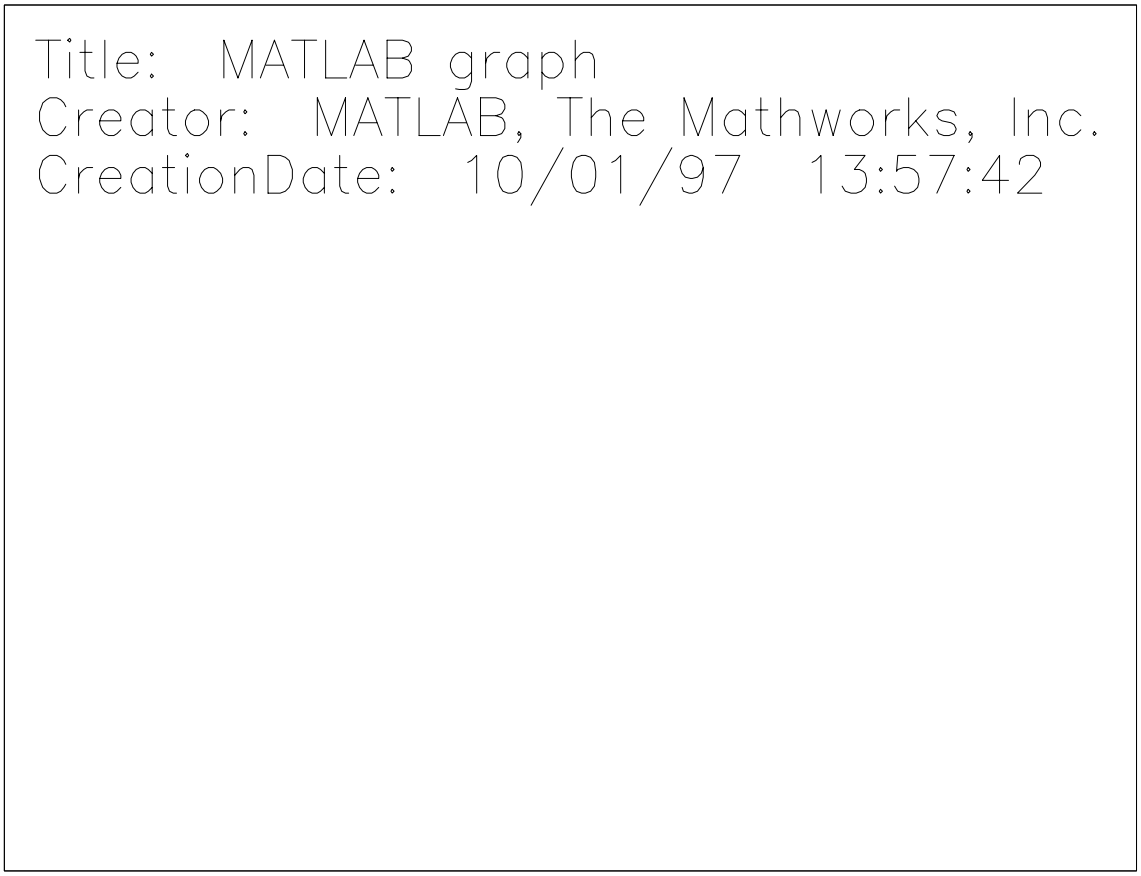

Figure 10: Summary of results of integration of steady core flow equations, with linear mass transfer model. Fast relaxation, $t = 100$ s. Inlet flow rate $q_0 = 10^{-5}$ ms^{-1}. Other parameters $p^{bubble} = 500$ psi, $K = 1.45 * 10^{-9}$ Pa^{-1}, $r_l^{ref} = 1000$ kg m^{-3}, $r_g^{ref} = 100$ kg m^{-3}, $\Lambda = 10^{-12}$ m^2 /Pa.s, $a = 0.3$.

Results with nucleation model

Using the nucleation model based mass transfer model, we obtain the results illustrated in Figures 11, 12 and 13. These Figures demonstrate the result of varying the inlet volume flow rate through the core, with all other parameters being held fixed. The input flow rate is small in Figure 11, medium in Figure 12, and large in Figure 13. The core length is adjusted in each simulation so that the pressure at the core exit is roughly the same in all cases. This means that simulations at high input flow rates are conducted on shorter domains than those at low flow rates.

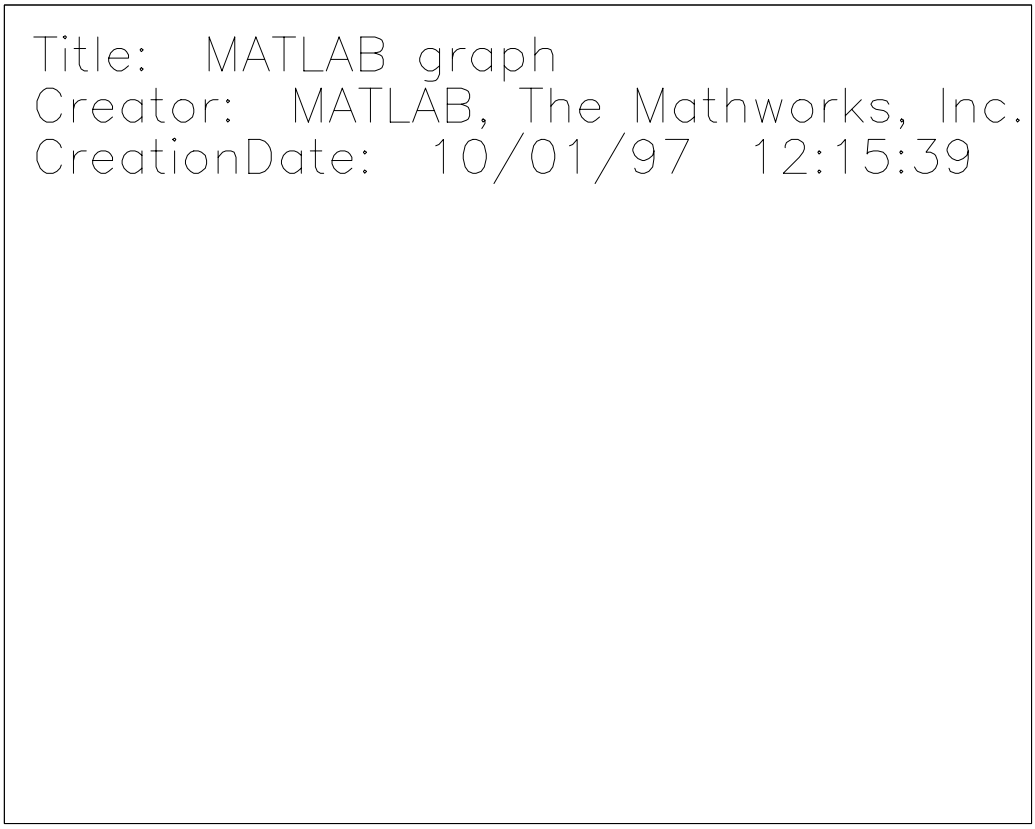

Figure 11: Summary of results of integration of steady core flow equations, with nucleation model based mass transfer terms. Inlet flow rate $q_0 = 10^{-7}$ ms^{-1}. At this very low flow rate, nucleation occurs in a small region near the core entrance. . Other parameters $p^{bubble} = 500$ psi, $K = 1.45*10^{-9}$ Pa^{-1}, $r_l^{ref} = 1000$ kg m^{-3}, $r_g^{ref} = 100$ kg m^{-3}, $p^{ref} = 1500$ psi, $\Lambda = 10^{-12}$ m^2 /Pa.s, $a = 0.3$, $f_{1,2} = 0.1$, $B = 10^5$ Pa, $C = 10^{10}$ m^{-3} s^{-1}, $D = 10^{-9}$ m^2 s^{-1}, $g = 0.02$ Nm.

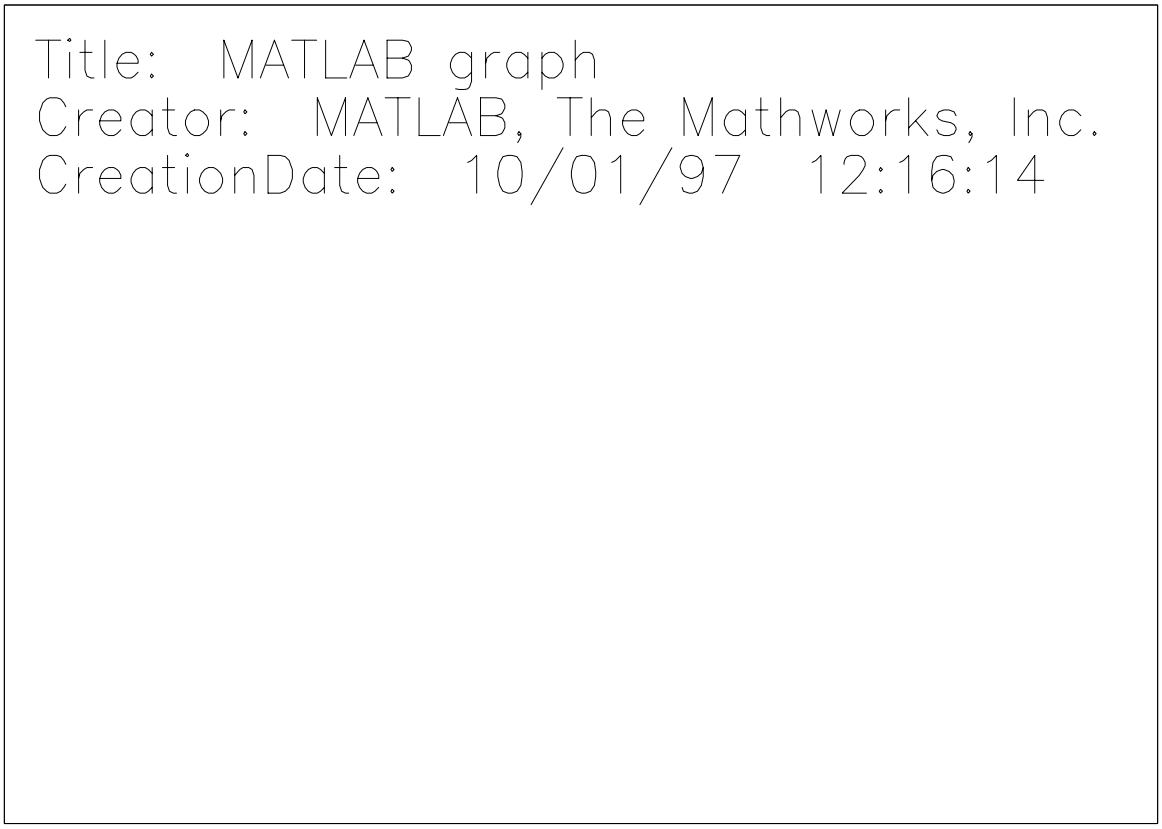

Figure 12: Summary of results of integration of steady core flow equations, with nucleation model based mass transfer terms. Inlet flow rate $q_0 = 10^{-5}\,\mathrm{ms}^{-1}$. This value is below the transition point, and nucleation again occurs only in a small region near the core entrance. Other parameters as previous figure.

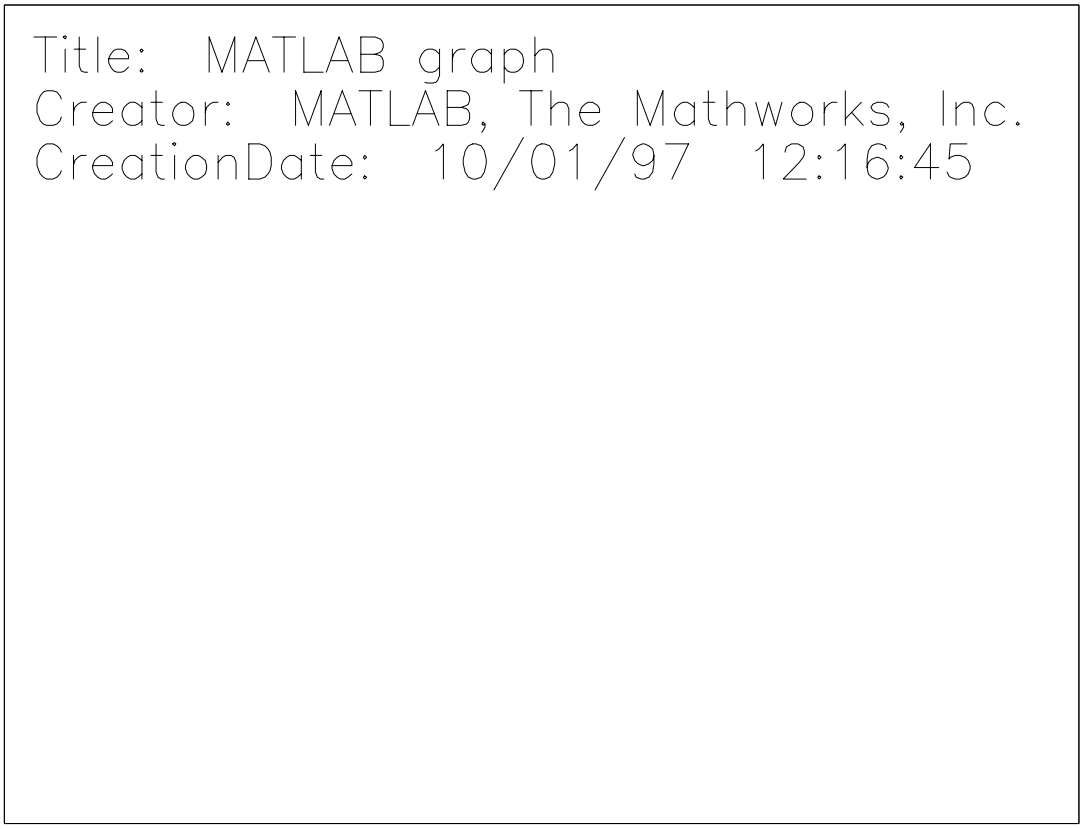

Figure 13: Summary of results of integration of steady core flow equations, with nucleation model based mass transfer terms. Inlet flow rate $q_0 = 10^{-4}$ ms^{-1}. This value is above the transition point, and nucleation is occurring everywhere within the core. Other parameters as previous figure.

As with the linear constitutive law, in all cases pressure falls and gas volume fraction and volume flow rate increase with distance into the core. There is a region near the core entrance through which the volume flow rate builds up to a roughly linear increase with distance. In the low flow rate cases of Figures 11 and 12 nucleation of bubbles occurs in a region near the core entrance, whereas in the high rate case of Figure 13, nucleation is occurring throughout the core. In all cases, outside a small region near the core entrance, the gas bubbles grow in size, by diffusion, with distance into the core. The average bubble size at core exit is smaller the larger the input volume flow rate. Although it is difficult to see from the Figures, the bubble volume fraction at cessation of nucleation is larger at high input flow rates than a low.

The existence of a transition in behaviour, between a zone of localised nucleation at low input flow rates, and nucleation occurring everywhere within the core at high input flow rates, is the key qualitative observation from these simulations. Secondary observations are the variation with input flow rate of average bubble size and of the bubble volume fraction at cessation of nucleation.

In order to investigate how the situation at the end of nucleation depends on the input flow rate to the core (or equivalently, on the mass flux through the zone of nucleation), a series of simulations were performed, varying the input flow rate over a range of values for which nucleation was localised. The results are recorded in Table 1. Quantities denoted with a tilde are values at cessation of nucleation, determined at the position at which N takes its maximum value. The supersaturation pressure, $\tilde{p}^{\sup er}$, is defined as the bubble point pressure less the pressure at the point of maximum N. The equilibrium volume

fraction, $\tilde{f}^{eq}$, is defined as the gas bubble volume fraction which would result if the gas-liquid mixture at the point of maximum N were allowed to relax to equilibrium at constant pressure. It is larger than the actual volume fraction at that point because the diffusive mass transfer process has not reached completion at the end of nucleation, and so the dissolved gas concentration is above its equilibrium value at the local pressure.

q_0 (m/s)	$\tilde{f}$	$\tilde{p}_{super}$ (Pa)	$\tilde{R}^{av}$ (m)	$\tilde{N}$ (m^{-3})	$\tilde{f}^{eq} = r_l K \tilde{p}^{super} / r_g$
10^{-7}	0.000113	$2.59*10^{4}$	$4.58*10^{-4}$	$2.80*10^{6}$	$3.74*10^{-4}$
10^{-6}	0.000244	$3.92*10^{4}$	$7.94*10^{-5}$	$1.16*10^{9}$	$5.69*10^{-4}$
10^{-5}	0.00108	$1.05*10^{5}$	$2.36*10^{-5}$	$1.94*10^{11}$	$1.53*10^{-3}$
$2*10^{-5}$	0.00257	$2.11*10^{5}$	$2.22*10^{-5}$	$5.65*10^{11}$	$3.06*10^{-3}$
$3*10^{-5}$	0.00496	$3.80*10^{5}$	$2.37*10^{-5}$	$8.95*10^{11}$	$5.51*10^{-3}$
$4*10^{-5}$	0.0115	$8.37*10^{5}$	$2.86*10^{-5}$	$1.70*10^{12}$	$1.01*10^{-2}$
$5*10^{-5}$	0.0243	$1.75*10^{6}$	$3.40*10^{-5}$	$1.40*10^{12}$	$2.54*10^{-2}$

Table 1: Variation of volume fraction, pressure, and bubble size and number, with input flow rate. Other parameters: $p^{bubble} = 500$ psi, $K = 1.45*10^{-9}$ Pa^{-1}, $r_l^{ref} = 1000$ kg m^{-3}, $r_g^{ref} = 100$ kg m^{-3}, $p^{ref} = 1500$ psi, $\Lambda = 10^{-12}$ m^2 /Pa.s, $a = 0.3$, $f_{1,2} = 0.1$, $B = 10^5$ Pa, $C = 10^{10}$ m^{-3} s^{-1}, $D = 10^{-9}$ m^2 s^{-1}, $g = 0.02$ Nm.

Two main conclusions can be drawn from these results. First, the average bubble size at cessation of nucleation decreases with increasing mass flux through the nucleation zone, at least until that mass flux is close to the value corresponding to transition to non-localised nucleation. Thus, the greater the mass flux through the nucleation zone, the smaller the bubbles that are created (and simultaneously, the more bubbles per unit volume of fluid). Secondly, the equilibrium volume fraction at cessation of nucleation increases with mass flux through the nucleation zone. Thus, the greater the mass flux through the nucleation zone, the larger the volume fraction of gas bubbles created, when converted to equilibrium conditions.

These observations will be used in the section below, where we consider unsteady and non-uniform depressurization flow in a core. In particular, at least when the volume flux through the core, or equivalently through the region in which nucleation is occurring is not too big, the process of nucleation and the initial, far from equilibrium, stages of bubble growth can be modelled by a jump in dispersed gas volume fraction. On one side of the jump there are no bubbles, and on the other, there is a finite bubble volume fraction, and the pressure and dissolved gas fraction are in approximate equilibrium. The gas volume fraction increases with distance from the nucleation zone, as pressure declines, due to flow, and gas comes out of solution and bubble volume fraction increases. The size of the volume fraction jump across the nucleation zone depends on the mass flux through the nucleation zone; this is illustrated in Table 1, where we see that the larger the flow rate, the larger the volume fraction jump. At higher flow rates, this picture, of localised nucleation, is no longer appropriate and a description in which bubbles are created throughout a finite region in space is necessary.

Simulation of flow during core depressurisation

In contrast to the situations studies in the two previous sections, the calculations of this section exhibit both non-uniformity and unsteadiness.

Consider one dimensional incompressible flow in a cylindrical porous permeable core of length L and cross sectional area A. Withdrawal occurs across the face of the core at $x = 0$, where the pressure is fixed in time and takes the value $p = p^{bubble} - \Delta p$. At $x = L$ we have a no flow boundary. For simplicity we shall only treat the case where all gas bubbles are trapped, so $\Lambda_{bl} = \Lambda_{bg} = 0$ (it is of course possible to set up the problem without making this assumption, but analytical progress cannot be made so easily because of non-linearities in the gas volume fraction transport equation). For simplicity, we also assume that $f^{l\to c}$, Λ_{lg} and Λ_{gl} are zero, and that capillary pressures are negligible. We shall assume that gas bubbles become connected, to form a continuous gas phase, immediately at the instant that $S_{gb} = S_{gb}^{*}$. This implies a form for $f^{b\to c}$ although we shall not state it explicitly, and will not investigate post-connection aspects of the flow here.

The basic transport equations are

$$p_l = p_{gb} = p_{gc} = p \tag{143}$$

$$\mathbf{q}_l = -\Lambda_{ll}\frac{\partial p}{\partial x} \tag{144}$$

$$\mathbf{q}_{gc} = -\Lambda_{gg}\frac{\partial p}{\partial x} \tag{145}$$

$$\mathbf{q}_{gb} = 0 \tag{146}$$

$$\mathbf{q}_{total} = -\left(\Lambda_{ll} + \Lambda_{gg}\right)\frac{\partial p}{\partial x} \tag{147}$$

$$-\frac{\partial}{\partial x}\left(\left(\Lambda_{ll} + \Lambda_{gg}\right)\frac{\partial p}{\partial x}\right) = \left(\frac{1}{r_g} - \frac{1}{r_l}\right) f^{l\to b} \tag{148}$$

$$\frac{\partial}{\partial t}\left(a\, S_l\right) + \frac{\partial}{\partial x}\left(\frac{\Lambda_{ll}}{\Lambda_{ll} + \Lambda_{gg}}\mathbf{q}_{total}\right) = -\frac{1}{r_l} f^{l\to b} \tag{149}$$

$$\frac{\partial}{\partial t}\left(a\, S_{gb}\right) = \frac{1}{r_g}\left(f^{l\to b} - f^{b\to c}\right) \tag{150}$$

$$S_{gc} = 1 - S_l - S_{gb} \tag{151}$$

$$\frac{\partial}{\partial t}\left(\alpha S_l \chi\right) + \frac{\partial}{\partial x}\left(\frac{\Lambda_{ll}}{\Lambda_{ll}+\Lambda_{gg}}\chi \mathbf{q}_{total}\right) = -\frac{1}{r_l} f^{l\to b} \tag{152}$$

$$\frac{\partial}{\partial t}(\alpha N) = n - c^{b\to c}. \tag{153}$$

The produced mass flow rates are

$$\mathbf{Q}_l = -r_l \Lambda_{ll} \left.\frac{\partial p}{\partial x}\right|_{x=0,t} \tag{154}$$

and

$$\mathbf{Q}_g = -r_g \Lambda_{gg} \left.\frac{\partial p}{\partial x}\right|_{x=0,t} \tag{155}$$

per unit area of outflow, and

$$R = \left.\frac{r_g \Lambda_{gg}}{r_l \Lambda_{ll}}\right|_{x=0,t} \tag{156}$$

is the ratio of the produced gas to produced liquid mass flow rates.

Finite mass transfer rate, with zero supersaturation required for initiation

We use the simple linear mass transfer law

$$f^{l\to g} = \begin{cases} \dfrac{\alpha S_l r_l (\chi - K p_l)}{t} & p_l < p^{bubble} \text{ or } S_{gb} > 0 \\ 0 & \text{otherwise} \end{cases}. \tag{157}$$

The pressure is taken to be equal to p^{bubble} initially, and the dissolved gas concentration to Kp^{bubble}, and so only the upper term in the brace is important.

Combining (149) and (152) we find (exactly) that

$$\alpha S_l \frac{\partial \chi}{\partial t} + \frac{\Lambda_{ll}}{\Lambda_{ll}+\Lambda_{gg}} q_{total} \frac{\partial \chi}{\partial x} = -\frac{1}{r_l}(1-\chi) f^{l\to b}. \tag{158}$$

This can be combined with (147) to read

$$\frac{r_l}{1-\chi}\left(\alpha S_l \frac{\partial \chi}{\partial t} - \Lambda_{ll}\frac{\partial p}{\partial x}\frac{\partial \chi}{\partial x}\right) = -f^{l\to b}, \tag{159}$$

and using (157) we have

$$\frac{\partial \chi}{\partial t} - \Lambda_{ll}\frac{1}{\alpha S_l}\frac{\partial p}{\partial x}\frac{\partial \chi}{\partial x} = -\frac{\chi - K p_l}{(1-\chi)t}. \tag{160}$$

Now, the second, convective, term on the left hand side of this equation may be neglected compared to the first, time derivative, term if $\left(\Lambda_{ll}\Delta p T/\alpha L^2\right) \ll 1$, where L and T are characteristic length and time scales for variation of the dissolved gas fraction. Since we expect the dissolve gas fraction to be closely related to the pressure field, and since, as we shall see below, the pressure field satisfies a diffusion equation, the quotient L^2/T may be equated to the diffusion coefficient for pressure, which is

$\Lambda_{ll} r_g / a K r_l$. Inserting this into the previous criterion, we find that the non-linear term may be neglected provided $\left(K\Delta p r_l / r_g\right) \ll 1$. But, this group is simply the volume fraction of gas that would be released, at equilibrium, were the pressure dropped by an amount Δp below the bubble point pressure. It is reasonable, and consistent with other approximations, to restrict attention to situations where this quantity is small. It is therefore legitimate to neglect the quadratic term in (160), and at the same time to linearize the RHS, giving

$$\frac{\partial x}{\partial t} \approx -\frac{x - K p_l}{t}. \tag{161}$$

If we now write

$$x'(x,t) = K p^{bubble} - x(x,t), \tag{162}$$

$$p'(x,t) = p^{bubble} - p(x,t), \tag{163}$$

then

$$\frac{\partial}{\partial x}\left(\left(\Lambda_{ll} + \Lambda_{gg}\right)\frac{\partial p'}{\partial x}\right) = \left(\frac{r_l}{r_g} - 1\right)\frac{a S_l\left(K p' - x'\right)}{t} \tag{164}$$

and

$$\frac{\partial x'}{\partial t} = -\frac{x' - K p'}{t}. \tag{165}$$

If we treat the mobilities as constant, and linearize the RHS of (164), which is an acceptable approximation if the liquid volume fraction is close to one, then these two equations can be solved by Laplace transformation in time. Denoting transformed quantities with a hat, we have

$$K\hat{p}' = (1 + t s)\hat{x}' \tag{166}$$

and

$$\left(\Lambda_{ll} + \Lambda_{gg}\right)\frac{d^2 \hat{p}'}{dx^2} = \left(\frac{r_l}{r_g} - 1\right)\frac{a\left(K\hat{p}' - \hat{x}'\right)}{t}. \tag{167}$$

Combining we have

$$\frac{d^2 \hat{p}'}{dx^2} - \frac{a K\left(r_l / r_g - 1\right)}{\Lambda_{ll} + \Lambda_{gg}}\frac{s}{1 + t s}\hat{p}' = 0, \tag{168}$$

the solution of which, decaying at infinity and satisfying the constant drawdown pressure boundary condition at the origin is

$$\hat{p}' = \frac{\Delta p}{s}\exp\left(-\sqrt{\frac{a K(r_l / r_g - 1)}{\Lambda}\frac{s}{(1 + t s)}}\,x\right). \tag{169}$$

Then,

$$\hat{x}' = \frac{K\Delta p}{s(1 + t s)}\exp\left(-\sqrt{\frac{a K(r_l / r_g - 1)}{\Lambda}\frac{s}{(1 + t s)}}\,x\right). \tag{170}$$

Now

$$\hat{Q} = -r_l \Lambda \left.\frac{d\hat{p}'}{dx}\right|_{x=0} = r_l \Lambda\ \Delta p\sqrt{\frac{a K(r_l / r_g - 1)}{\Lambda}\frac{1}{s(1 + t s)}}, \tag{171}$$

so [Abramowitz 29.3.49]

$$Q(t) = r_l \Lambda \ \Delta p \sqrt{\frac{a\,K(r_l / r_g - 1)}{\Lambda\ t}}\exp(-t/2t)I_0(t/2t)\,, \tag{172}$$

which for large time is approximately

$$Q(t) \approx r_l \Lambda \ \Delta p \sqrt{\frac{a\,K(r_l / r_g - 1)}{\Lambda}}\frac{1}{\sqrt{p\,t}}\left(1+\frac{t}{4t}\right) \tag{173}$$

and for small time is approximately

$$Q(t) \approx r_l \Lambda \ \Delta p \sqrt{\frac{a\,K(r_l / r_g - 1)}{\Lambda}}\frac{1}{\sqrt{t}}\ . \tag{174}$$

The produced flow rate decays algebraically at large times, and is finite at small times.

Turning now to the bubble volume fraction, we have

$$a\ \frac{\P S_{gb}}{\P t} = a\ \frac{r_l}{r_g}\left(1-S_{gb}\right)\left(Kp'-x'\right) \tag{175}$$

If we write $-\log\left(1-S_{gb}\right) = \left(r_l K\Delta p / r_g\right)y$, then

$$\frac{\P y}{\P t} = \frac{Kp'-x'}{K\Delta p} \tag{176}$$

which leads, using the Laplace transform solutions already found, immediately to

$$\hat{y} = \frac{1}{s(1+ts)}\exp\left(-\sqrt{\frac{a\,K(r_l / r_g - 1)}{\Lambda}\frac{s}{(1+ts)}}x\right). \tag{177}$$

Now

$$\hat{y}(0,s) = \frac{1}{s(1+ts)} \tag{178}$$

and so

$$y\ (0,t) = 1-e^{-t/t}\ . \tag{179}$$

For small dispersed gas volume fractions $S_{gb} \approx \left(r_l K\Delta p / r_g\right)y$, and so the dispersed gas volume fraction at the core exit tends exponentially towards a finite value.

It is also of interest to consider the time behaviour of the supersaturation (at a fixed position in the core), and the time rate of change of pressure. The transforms of these quantities are

$$\hat{s}_l = \frac{K\Delta p t}{(1+ts)}\exp\left(-\sqrt{\frac{a\,K(r_l / r_g - 1)}{\Lambda}\frac{s}{(1+ts)}}x\right) \tag{180}$$

and

$$\overline{\frac{\partial p}{\partial t}} = -\Delta p \exp\left(-\sqrt{\frac{a\,K(r_l / r_g - 1)}{\Lambda} \frac{s}{(1+ts)}}\, x \right) . \qquad (181)$$

The Laplace transforms of these, and the other functions, may be inverted numerically to give solutions in the time domain. The method of [de Hoog] works well. Note that all the parameters can be scaled out of the problem if we set $x^* = x / \sqrt{\Lambda t / Ka\,(r_l / r_g - 1)}$, $t^* = t / t$, $p^{*\prime} = p'/\Delta p$, $x^{*\prime} = x'/K\Delta p$, $s_l^* = s_l / K\Delta p$. Plots of various solution quantities are given in the following Figures.

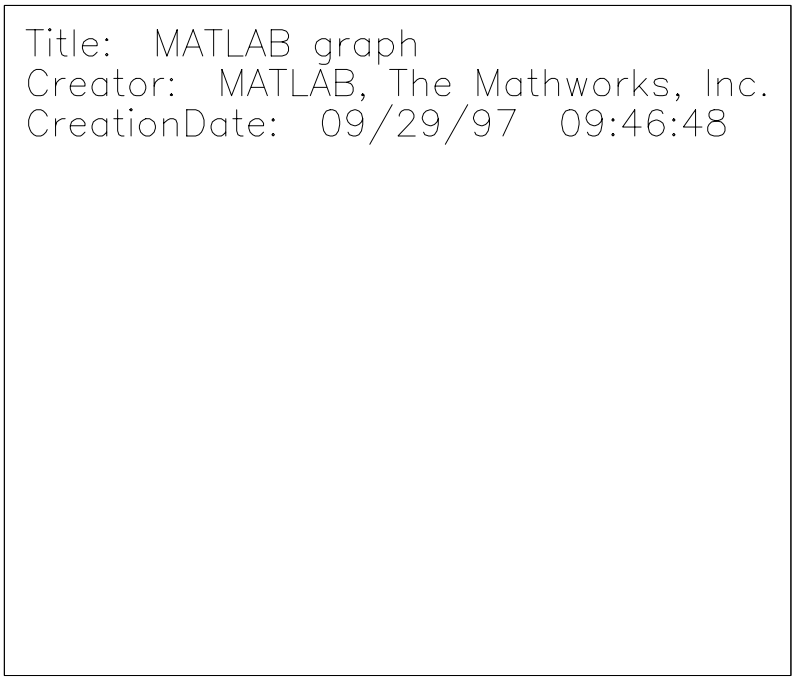

Figure 14: $p^{*\prime}(x^*, t^*)$ computed by numerical inversion of the Laplace transform solution, for $t^* = 0.1, 0.22, 0.46, 1, 2.2, 4.6, 10, 22, 46, 100$.

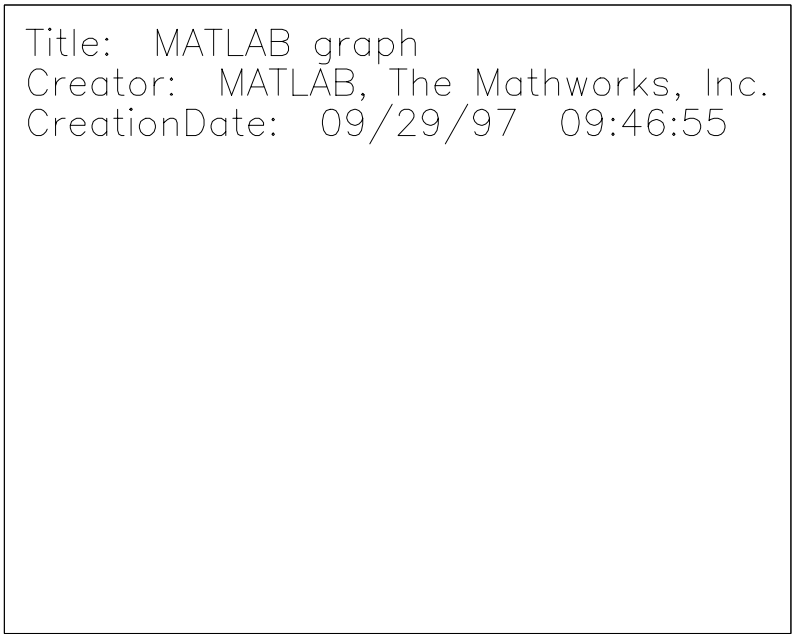

Figure 15: $p^{*\prime}(x^* / t^{*1/2}, t^*)$ computed by numerical inversion of the Laplace transform solution, for $t^* = 0.1, 0.22, 0.46, 1, 2.2, 4.6, 10, 22, 46, 100$. Note that the solution exhibits similarity scaling at large dimensionless time, but not at small.

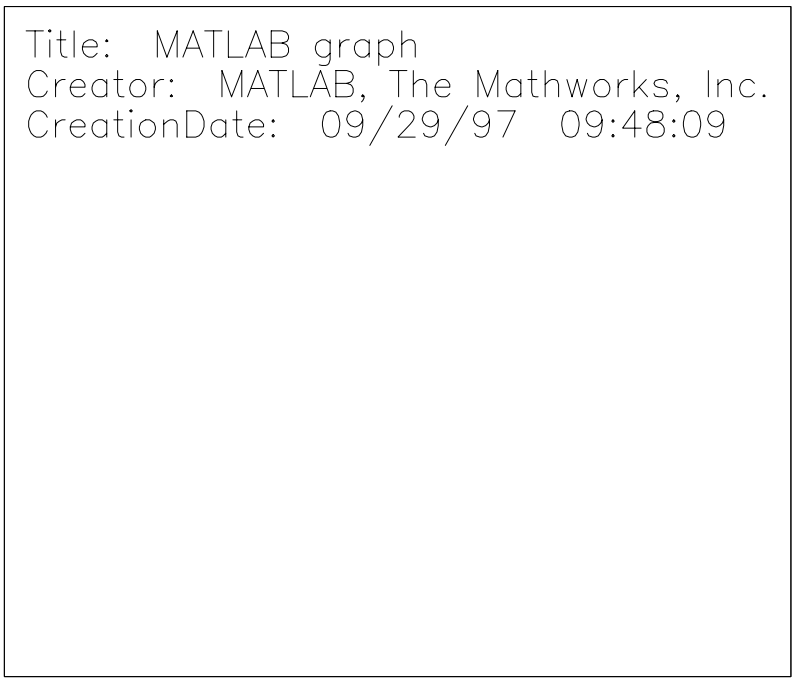

Figure 16: The scaled dispersed gas volume fraction, $y(x^*, t^*)$, for $t^* = 0.1, 0.22, 0.46, 1, 2.2, 4.6, 10, 22, 46, 100$.

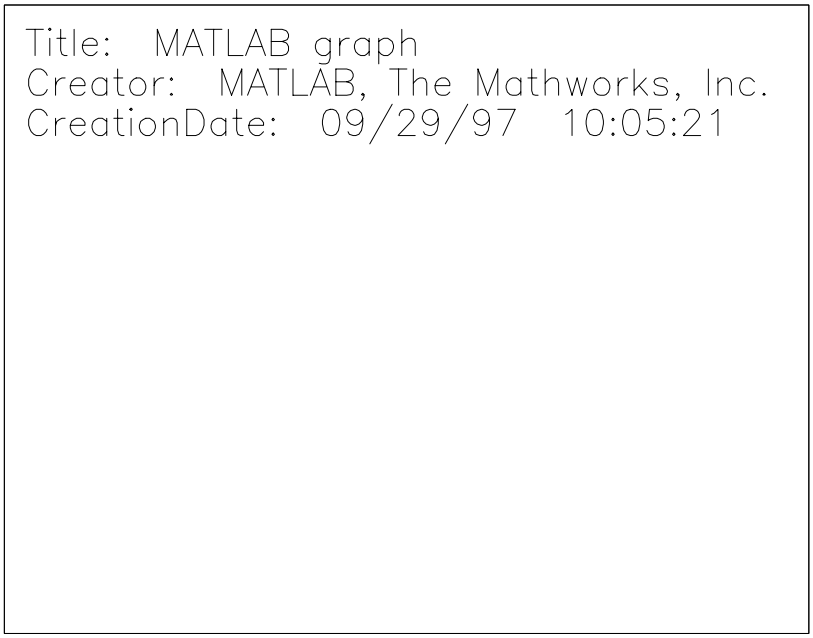

Figure 17: The supersaturation, $s_l(x^*,t^*)$ at $x^* = 1{,}5$ as a function of t^*.

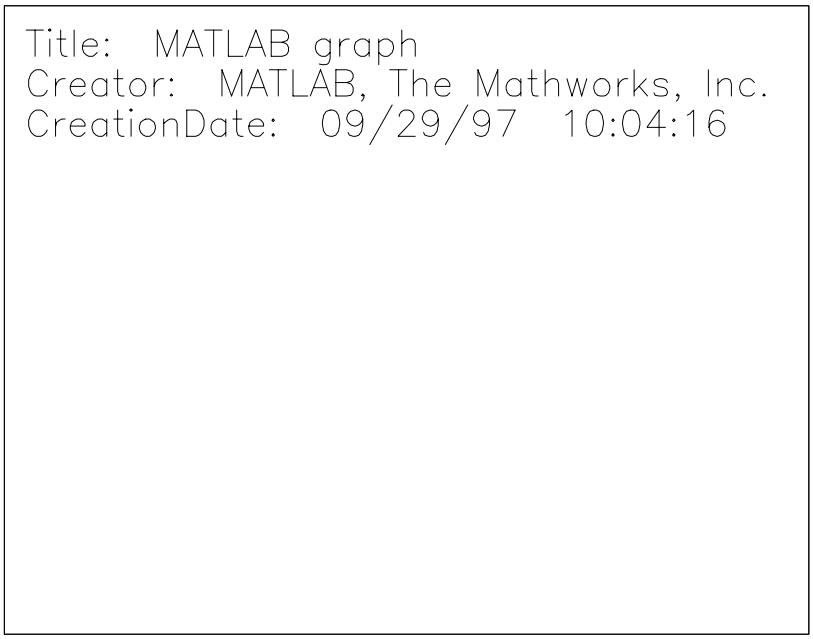

Figure 18: The time rate of change of pressure, $dp^*'/dt^*(x^*,t^*)$ at $x^* = 1{,}5$ as a function of t^*.

The solution has the expected features. The pressure disturbance propagates into the core, at large times the disturbance has similarity scaling and is essentially diffusive, whereas at smaller times, the pressure disturbance propagates somewhat faster than the diffusive solution (the case $t = 0$). There are no sharp fronts, nor is there any hint of frontal advance at a fixed velocity (this distinguishes this model from another, in which a different constitutive equation for mass transfer is assumed, and which predicts that pressure disturbances satisfy a telegraph equation). The dispersed gas volume fraction increases

everywhere with time, and again, the disturbance propagates into the core, approaching a form with similarity scaling at large times. The supersaturation is initially large near the core exit, but decreases in magnitude with time. The further we go into the core, the smaller the peak supersaturation, and the later in time it occurs. At each location, the scaled supersaturation decays to zero as time increases. The same statements are true of the rate of change of pressure. Thus, we can say that if bubble nucleation were driven by this pressure history, and if the supersaturation to initiate nucleation were vanishingly small, near the core entry bubbles would be created in conditions of large rates of pressure change and large supersaturation, and that both of these quantities would decay as we moved further into the core.

The crucial feature of solutions to this problem is that the pressure disturbance is non-zero (but small) at all points in the core, immediately flow is initiated (in some sense, the speed of propagation of diffusive disturbances is infinite). Because the bubble volume fraction and pressure are directly proportional, the gas bubble volume fraction is finite everywhere within the core at all times after the initial instant also. There are no propagating fronts or discontinuities.

Rapid mass transfer, with finite supersaturation required for initiation

We assume that a finite supersaturation is required for bubbles to be nucleated, and that the time scale $t^{l\to b}$ for post-nucleation mass transfers of gas from dissolved to bubble form is very small compared to any other time scale of the flow process. To model bubble nucleation and initial non-equilibrium growth, we assume that the dissolved gas mass fraction jumps from its initial value Kp^{bubble} down to $K(p^{bubble} - p^{\sup er})$ instantaneously, at the moment at which the pressure first falls below $p^{bubble} - p^{\sup er}$. Gas component mass conservation then implies that at the same instant the gas bubble volume fraction jumps from zero up to

$$f_0 = Kp^{\sup er} r_l / r_g \ . \qquad (182)$$

As was argued in the studies of steady flow through a core reported above, localised nucleation occurs provided the flow rate through the nucleation zone is not too large. Thus, the model of the present sub-section is valid for drawdowns that are not too big, or at late times for which frontal advance velocities have fallen to a low value. The number of bubbles created per unit volume is $N_0 = f_0 / V$, where V is the initial volume of each nucleated bubble, a further quantity which must be prescribed. The temporal rate of creation of bubbles clearly depends on the rate at which fluid passes across the moving surface on which the pressure equals $p^{bubble} - p^{\sup er}$. For that reason, the explicit expression for n will contain the velocity at which that nucleation pressure iso-surface propagates into the rock, and so it is simpler, for now, to simply state the jump conditions, as above, rather than give a functional form for n.

Now, because we have assumed that $t^{l\to b}$ is very small, and because we always have pressures below the initial saturation pressure, $x \approx Kp$ when $p < p^{bubble} - p^{sup\,er}$, and so $\partial x/\partial t \approx K\,\partial p/\partial t$ and $\partial x/\partial x \approx K\,\partial p/\partial x$ then. Prior to bubble nucleation, the dissolved gas mass fraction does not change in time; when $p > p^{bubble} - p^{sup\,er}$, $\partial x/\partial t = \partial x/\partial x = 0$. Now, (160) can be used to used to substitute for the source term on the RHS of (148). Making this substitution, and using the expressions linking pressure and composition changes, we obtain

$$\frac{\partial}{\partial x}\left(\left(\Lambda_{ll}+\Lambda_{gg}\right)\frac{\partial p}{\partial x}\right)=\left(\frac{1}{r_g}-\frac{1}{r_l}\right)\frac{r_l}{1-x}\left(a\,S_l\,\frac{\partial x}{\partial t}-\Lambda_{ll}\,\frac{\partial p}{\partial x}\frac{\partial x}{\partial x}\right)\approx$$

$$\begin{cases}\left(\dfrac{1}{r_g}-\dfrac{1}{r_l}\right)\dfrac{r_l}{1-x}K\left(a\,S_l\,\dfrac{\partial p}{\partial t}-\Lambda_{ll}\left(\dfrac{\partial p}{\partial x}\right)^2\right) & p < p^{bubble} - p^{sup\,er}\\ 0 & p > p^{bubble} - p^{sup\,er}\end{cases} \qquad (183)$$

which is a diffusion-like equation for the pressure, with non constant coefficients which depend on the solution of the volume fraction equations. Solutions on either side of the nucleation zone are linked by appropriate jump or continuity conditions. At the core exit, $x = 0$, we have

$$p = p^{bubble} - \Delta p \qquad (184)$$

while at the sealed end face of the core, $x = L$, we have

$$-\left(\Lambda_{ll}+\Lambda_{gg}\right)\frac{\partial p}{\partial x} = 0 \quad . \qquad (185)$$

At the initial instant the pressure within the core must also be prescribed, and we take

$$p(x,0^+) = p^{bubble} . \qquad (186)$$

As we shall remark below, neglect of liquid compressibility causes mathematical problems associated with the satisfaction of initial conditions on pressure, and in fact, we shall not directly make use of this condition in the solution presented below.

Conditions at the point at which nucleation occurs also require special consideration. Denote the position at which $p = p^{bubble} - p^{sup\,er}$ as $x = X(t)$, and write $dX/dt = U$. If we transform to a system of coordinates moving with $X(t)$, then integrating the mixture mass conservation equation

$$a\,\frac{\partial}{\partial t}\left(r_l S_l + r_g S_g\right)+\frac{\partial}{\partial x}\left(r_l\,\frac{\Lambda_{ll}}{\Lambda_{ll}+\Lambda_{gg}}\mathbf{q}_{total}\right)=-f^{b\to c}, \qquad (187)$$

which is obtained by adding (149) and (150) across the point at which nucleation occurs, and using (147), yields

$$a\,U f_0\left(r_l - r_g\right) = -r_l\Lambda_{ll}\frac{\partial p}{\partial x}(X^+,t)+r_l\left(\Lambda_{ll}+\Lambda_{gg}\right)\frac{\partial p}{\partial x}(X^-,t) \qquad (188)$$

(assuming that no bubble coalescence occurs at nucleation). This equation links the speed at which the bubble containing region propagates into the core to the changes in pressure gradient and bubble volume fraction at the nucleation front.

Turning now to the equations governing volume fractions, using (160) and the approximate relationships between composition and pressure derivatives to substitute for the mass transfer term in the (exact) bubble volume fraction evolution equation (150), we obtain

$$a\,\frac{\P S_{gb}}{\P t} \approx \frac{1}{r_g}\begin{cases} -K\dfrac{r_l}{(1-x)}\left(a\,S_l\,\dfrac{\P p}{\P t} - \Lambda_{ll}\left(\dfrac{\P p}{\P x}\right)^2\right) - f^{\,b\to c} & p < p^{bubble} - p^{sup\,er} \\ 0 & p > p^{bubble} - p^{sup\,er} \end{cases} . \qquad (189)$$

At the point at which $p = p^{bubble} - p^{sup\,er}$, S_{gb} jumps from zero to f_0. Under circumstances when the term quadratic in the pressure gradient can be neglected, and $x \ll 1$, $S_l \approx 1$ and $S_{gb} < S_{gb}^*$, we may integrate this equation to obtain

$$S_{gb}(x,t) \approx \begin{cases} f_0 + \dfrac{r_l K}{r_g}\left(p^{bubble} - p^{sup\,er} - p(x,t)\right) & p > p^{bubble} - p^{sup\,er} \\ 0 & p > p^{bubble} - p^{sup\,er} \end{cases} . \qquad (190)$$

Now, using the definition of f_0, we may rewrite this expression as

$$S_{gb}(x,t) \approx \frac{r_l K \Delta p}{r_g}\begin{cases} \dfrac{p^{bubble} - p(x,t)}{\Delta p} & p > p^{bubble} - p^{sup\,er} \\ 0 & p > p^{bubble} - p^{sup\,er} \end{cases} \qquad (191)$$

which shows the direct relationship between gas volume fraction and pressure perturbation. The quantity $r_l K \Delta p / r_g$ is the gas bubble volume fraction that would be attained in equilibrium if the pressure were dropped to $p^{bubble} - \Delta p$. Dropping the quadratic term in the source term of the volume fraction evolution equation is justified by the same kind of argument as given earlier; this term is relatively smaller than those retained by a factor of order $r_l K \Delta p / r_g$. That said, neglecting this term is not a completely benign approximation, since it is always positive, and it models the increase of gas volume fraction at each point caused by trapping of gas bubbles evolving from supersaturated fluid moving through. Neglecting this term means that we do not capture this effect, although changes in volume fraction due to pressure changes are captured.

In the liquid volume fraction equation, the convective term may be expanded to give

$$\frac{\P}{\P t}\left(a\,S_l\right) + \mathbf{q}_{total}.\nabla\left(\frac{\Lambda_{ll}}{\Lambda_{ll}+\Lambda_{gg}}\right) = -\frac{1}{r_l}\,f^{\,l\to b} - \frac{\Lambda_{ll}}{\Lambda_{ll}+\Lambda_{gg}}\nabla.\mathbf{q}_{total} \qquad (192)$$

and using the pressure equation (148) this may be written

$$\frac{\P}{\P t}\left(a\,S_l\right) + \mathbf{q}_{total}.\nabla\left(\frac{\Lambda_{ll}}{\Lambda_{ll}+\Lambda_{gg}}\right) = -\frac{1}{r_l}\,f^{\,l\to b} - \frac{\Lambda_{ll}}{\Lambda_{ll}+\Lambda_{gg}}\left(\frac{1}{r_g} - \frac{1}{r_l}\right)f^{\,l\to b} . \qquad (193)$$

Substituting for the transfer term, we obtain

$$\frac{\P}{\P t}\left(a\,S_l\right) + q_{total}\,\frac{\P}{\P x}\left(\frac{\Lambda_{ll}}{\Lambda_{ll}+\Lambda_{gg}}\right) \approx$$

$$\begin{cases} K\dfrac{1}{1-x}\left(a\,S_l\,\dfrac{\P p}{\P t} - \Lambda_{ll}\left(\dfrac{\P p}{\P x}\right)^2\right)\dfrac{\dfrac{r_l}{r_g}\Lambda_{ll} + \Lambda_{gg}}{\Lambda_{ll}+\Lambda_{gg}} & p < p^{bubble} - p^{sup\,er} \\ 0 & p < p^{bubble} - p^{sup\,er} \end{cases} . \qquad (194)$$

At the point at which $p = p^{bubble} - p^{super}$, S_l jumps down by an amount f_0, in response to the creation of bubble volume through nucleation. If we now drop the quadratic terms (which means that we fail to capture the decrease of liquid fraction due to gas trapping), and treat the mobility terms on the RHS as piece-wise constants (in time), the previous equation may be integrated to give

$$\log\left(S_l(x,t)\right) \approx \begin{cases} K\dfrac{\dfrac{r_l}{r_g}\Lambda_{ll} + \Lambda_{gg}}{\Lambda_{ll} + \Lambda_{gg}}\left(p(x,t) - p^{bubble} - p^{super}\right) & p < p^{bubble} - p^{super} \\ 0 & p > p^{bubble} - p^{super} \end{cases} \qquad (195)$$

when $x \ll 1$. From this, or the basic evolution equation, we see that the liquid saturation responds strongly to changes in pressure when no connected gas is present, but once connected gas (with sufficiently high mobility) exists, the effect of pressure changes on liquid saturation changes falls by a factor of $O(r_g / r_l)$. This is reflection of the fact that once gas becomes connected, liquid production rates fall dramatically.

The connected gas volume fraction follows at once, because the sum of the volume fractions must be unity.

The upshot of these manipulations is that the saturation dependent coefficients in the pressure diffusion equation (183) can all be written as functions of pressure (at least in circumstances where the dependence of mobility on saturation is simple, that is, not hysteretic). Thus, provided the various approximations are valid, only a single non-linear diffusion equation, for p, must be solved in order for the system behaviour to be completely calculated.

Solving the above system of equations requires numerical integration, but if we are prepared to take p^{super} and f_0 constant in time and independent of the mass flux through the nucleation zone, then an analytical solution is possible. There is no real, rigourous, justification for this simplification, for in the previous studies of nucleation during steady flow through a core, the solutions indicated clearly that the volume fraction created at nucleation was an increasing function of the mass flux through the nucleation zone. The present approximation can be justified only in so far as it is a route to creating illustrative solutions which give some indication of the structure and properties of this non-linear unsteady core flow problem.

We now solve for the pressure distribution, taking $p^{super} > 0$ but less than Δp, and constant. In $L > x > X(t)$ the pressure field satisfies

$$\frac{\partial}{\partial x}\left(\left(\Lambda_{ll} + \Lambda_{gg}\right)\frac{\partial p}{\partial x}\right) = 0 \qquad (196)$$

and $\left(\Lambda_{ll} + \Lambda_{gg}\right)\partial p / \partial x(L,t) = 0$. Since $\Lambda_{ll} + \Lambda_{gg}$ is constant (it depends only on the gas volume fraction, which is zero), the solution in this region is

$$p(x,t) = \text{constant} \qquad (197)$$

(valid until $X(t)$ becomes equal to L). This statement conceals a problem, to do with the neglect of compressibility and the requirement to satisfy initial conditions; in reality, the liquid above the bubble point is slightly compressible, and there is a pressure profile ahead of the nucleation front, through which the pressure rises from a value set by the nucleation process to the initial condition value at great distances. Because we are neglecting compressibility, there is no mechanism in the present calculation to

capture this pressure adjustment process, and this missing feature manifests itself as the requirement that the pressure ahead of the nucleation front is constant and, by spatial continuity of pressure, equal to the pressure just behind the nucleation front, which is different to the initial condition pressure. We shall not pursue this point further, beyond saying that it is a purely mathematical difficulty that can be removed if account is taken of liquid compressibility.

If we now drop the quadratic term in (183), in $0 < x < X(t) < L$, the pressure satisfies

$$\frac{\partial}{\partial x}\left(\left(\Lambda_{ll} + \Lambda_{gg}\right)\frac{\partial p}{\partial x}\right) = \left(\frac{1}{r_g} - \frac{1}{r_l}\right)\frac{\alpha S_l r_l}{1-x} K \frac{\partial p}{\partial t} \qquad (198)$$

with $p(0,t) = p^{bubble} - \Delta p$ and $p(X^-,t) = p^{bubble} - p^{super}$. At $x = X(t)$ we must have

$$\alpha \frac{dX}{dt} f_0 \left(r_l - r_g\right) = r_l \left(\Lambda_{ll} + \Lambda_{gg}\right)\frac{\partial p}{\partial x}(X^-,t), \qquad (199)$$

since the pressure gradient ahead of the front vanishes, and this expression is an ordinary differential equation for $X(t)$. Together, (198) and (199), with the relevant boundary and initial conditions, specify a Stefan-type problem for p. It is known that such problems possess similarity solutions in the variable $h = x / t^{1/2}$ (at least, in this case, until $X(t)$ becomes equal to L), and in fact, the similarity solution still exists if the quadratic terms are retained, although integration in terms of elementary functions would then not be possible. Had we not taken p^{super} or f_0 constant, then the similarity solution would not exist, and numerical integration would be necessary at this stage.

If we approximate the mobilities to be constant, and take $S_l / 1-x \approx 1$ and $L \to \infty$, then it is straightforward to see that the solution to the Stefan problem is

$$X(t) = 2\Xi(Dt)^{1/2} \qquad (200)$$

and

$$p(x,t) = (p^{bubble} - \Delta p) + (\Delta p - p^{super})\begin{cases} \dfrac{1 - \mathrm{erfc}\left(\dfrac{h}{2D^{1/2}}\right)}{1 - \mathrm{erfc}(\Xi)} & x < X(t) \\ 1 & x > X(t) \end{cases} \qquad (201)$$

where $\mathrm{erfc}(x) = \dfrac{2}{\sqrt{\pi}}\int_x^\infty e^{-y^2} dy$, $\mathrm{erfc}(0) = 1$, $\mathrm{erfc}(\infty) = 0$, $d\,\mathrm{erfc}(x)/dx = -2e^{-x^2}/\sqrt{\pi}$,

$$D = \frac{\Lambda_{ll} + \Lambda_{gg}}{\alpha K\left(\dfrac{r_l}{r_g} - 1\right)}, \qquad (202)$$

and Ξ satisfies the transcendental equation

$$\alpha \Xi D^{1/2} f_0 (r_l - r_g) = r_l (\Lambda_{ll} + \Lambda_{gg})(\Delta p - p^{super})\frac{e^{-\Xi^2}}{1 - \mathrm{erfc}(\Xi)} D^{-1/2} \qquad (203)$$

which may be re-written as

$$\frac{p^{\sup er}}{\Delta p - p^{\sup er}}\Xi = \frac{e^{-\Xi^2}}{1-\mathrm{erfc}(\Xi)}. \qquad (204)$$

From this expression it is easy to see, by curve sketching, that a unique positive solution for Ξ exists, which decreases as $p^{\sup er}$ increases. The produced liquid mass flow rate is

$$Q_l = \frac{r_l \Lambda_{ll}(\Delta p - p^{\sup er})}{\sqrt{p}} \frac{1}{1-\mathrm{erfc}(\Xi)} (Dt)^{-1/2} \qquad (205)$$

per unit area of core. When $p^{\sup er}$ is zero, the problem for pressure reduces to straightforward diffusion, with solution

$$p(x,t) = p^{bubble} - \Delta p\, \mathrm{erfc}\left(\frac{h}{2D^{1/2}}\right). \qquad (206)$$

Figure 19 shows the scaled volume fraction distribution, or pressure perturbation, predicted by the solution to this Stefan problem.

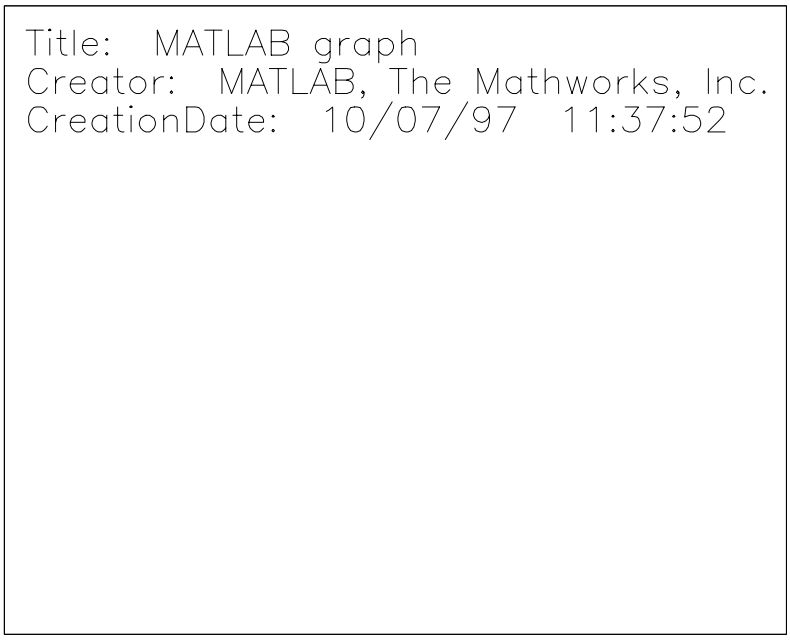

Figure 19: Scaled dispersed gas volume fraction (closely related to pressure perturbation) for Stefan solution. Solid curve, $\Delta p / p^{\sup er} = 1.5$; dotted curve, $\Delta p / p^{\sup er} = 20$; dashed curve, solution of diffusion equation, $\Delta p / p^{\sup er} = \infty$.

The crucial feature of the solution to the problem in this case is that the region containing bubbles is limited in extent, and the point dividing this region of finite gas volume fraction from that containing no free gas moves with finite speed into the core. There is a jump discontinuity in gas bubble fraction, and a discontinuity in pressure gradient. Gas bubbles appear at any given point in the core a strictly finite time after flow is initiated; they are not present everywhere, from initial instant. This is in sharp contrast to the situation which was analysed in the previous sub-section. These statements remain true if $p^{\sup er}$ is not taken to be constant, but varies with U.

The ratio of the produced liquid flow rates at finite to zero supersaturation is

$$\frac{Q_l(p^{\sup er})}{Q_l(0)} = \frac{\Delta p - p^{\sup er}}{\Delta p} \frac{1}{1-\mathrm{erfc}(\Xi)} . \qquad (207)$$

It is straightforward to solve (204) and then evaluate the RHS of (207), and we then find that the ratio of production rates is a smoothly decreasing function of $p^{\sup er} / \Delta p$, tending to 1 as $p^{\sup er} / \Delta p \to 0$ and to 0 as $p^{\sup er} / \Delta p \to 1$. Thus, the produced flow rate becomes lower as the supersaturation level required for nucleation increases, at least when the mobilities are unaffected by the changing nucleation conditions.

It is of course possible that the mobilities are affected by nucleation conditions; we might imagine, for example, that more but smaller bubbles are created at higher supersaturation levels, which in turn might lead to the liquid mobility being increased relative to that associated with nucleation of larger bubbles at lower supersaturations. Unfortunately, there is no observational evidence, one way or the other, on this matter. If the mobilities were changed, then the production rates would change too. The produced fluid flow rate ratio, when mobilities are supersaturation dependent, may be written as

$$\frac{Q_l(p^{\sup er})}{Q_l(0)} = \frac{\Delta p - p^{\sup er}}{\Delta p} \frac{\Lambda_{ll}(p^{\sup er})}{\Lambda_{ll}(0)} \sqrt{\frac{D(0)}{D(p^{\sup er})}} \frac{1}{1-\mathrm{erfc}(\Xi)} , \qquad (208)$$

which increases as the ratio $\Lambda_{ll}(p^{\sup er}) / \Lambda_{ll}(0)$ increases.

Summary and Conclusions

A consistent two component, three phase, framework has been presented to describe the flow of a foamy crude in a porous medium, in which both gas bubbles and connected gas are present. By suitable choice of a mobility term, the bubbles may be trapped, may move with the liquid, or do anything in between. Because connected gas is treated within the framework, computations can be pursued beyond the point at which gas bubbles are so numerous that they become connected, without the need for any special treatment. Of course, in order that this may be done sensibly, additional constitutive functions must be defined. The governing equations are more complicated that those used previously, and for many practical problems the added complexity is unnecessary, and can be avoided by dropping terms representing unimportant effects (e.g. capillarity).

The Darcy law with cross terms formulation may be an appropriate way to include finite capillary number effects into the model. When flow rates, or more interestingly for present purposes, fluid viscosities are large, viscous forces may become larger than the capillary forces which were assumed to control the arrangements of the phases within the pore space. If this happens, then the local geometry of the fluids changes, and elements of fluid which might have been trapped become able to flow. Large scale consequences include a flow rate dependence of critical saturations, and flow of regions of fluid without large scale connectivity.

Constitutive functions describing mass transfer of gas between free and dissolved forms must be supplied in order to close the model. Two constitutive descriptions for dissolved to bubble mass transfer were presented and investigated above. The first of these is a simple linear first order kinetic model, in which the rate of transfer is proportional to the difference between the current dissolved gas contribution and that which would obtain in equilibrium at the current pressure. This model does not contain bubble size or number as a parameter, and so makes no prediction about these, potentially important and interesting quantities. The second mass transfer model is based on heterogeneous nucleation theory, and is strongly non-linear, requiring a finite supersaturation before creation of bubbles can commence, and making the rate of mass transfer into already existing bubbles depend on the size of these bubbles as well as on the departure of dissolved gas fraction from its equilibrium value. The model predicts values for the average bubble size, and the number of bubbles per unit fluid volume. Both models produce plausible results in simulations of sand pack depressurization or steady flow through a core. However only the nucleation theory based model can reproduce the pressure undershoot and recovery which is observed in constant volume expansion rate sand pack depressurization tests. This is highly suggestive of the need for a non-linear description for the mass transfer kinetics; whether the full nucleation model framework is necessary, or whether instead a simpler description, in which perhaps the time scale for mass transfer is made a function of the bubble volume fraction and the supersaturation, is possible, is a question that remains to be investigated.

It is true that the theory of nucleation in porous media is not well developed, and is certainly an area needing much further research. Also, numerical values of some of the parameters appearing in the nucleation model are hard, or perhaps impossible, to measure independently (for example the shape factors which account for the consequences of nucleation of non-spherical bubbles on solid surfaces seem to me to be determinable only by adjusting their values until the nucleation model produces sensible results). For this reason, and also because of the large number of parameter values that must be supplied in order to use the nucleation model, I do not feel that it offers a useful *practical* simulation model, although it is valuable as a tool for understanding mechanism. Something simper, and more closely linked to performable laboratory measurements, is necessary if we are to predict the outcome in field situations. Again, this is a question remaining to be investigated. I do believe, however, that the general behaviours predicted by the nucleation model, for example a supersaturation threshold for commencement of nucleation and a rapidly increasing rate of mass transfer with bubble size or volume fraction, are characteristic of the mass transfer process and are necessary to be captured in a mass transfer model for

FHC. Furthermore, I believe that any model that captures these features will, when used within the full transport equation framework, generate plausible behaviour in simulations of experiment.

The model is used to investigate three problems, all of which correspond to experimental situations that can be (or have already been) set up in the laboratory. The first problem is depressurization, either at controlled volume expansion rate or at controlled rate of pressure decline, of an initially gas saturated oil sample within a sand pack, at rates sufficiently slow that the pressure and other quantities may all be assumed spatially uniform within the sand pack. The second problem is steady one dimensional flow of initially gas saturated oil, at prescribed input volume flow rate, through a core. The last problem is the transient and spatially non-uniform one dimensional flow generated within an initially sealed FHC saturated core when one end is suddenly opened to flow, the pressure at that end being held constant in time, at a value below the bubble point. The first two problems reduce to systems of non-linear ordinary differential equations, which can be solved easily on a desk top PC using packaged solver routines. The third problem leads to a set of partial differential equations. These are soluble by Laplace transformation when the linear mass transfer law is used and pressure drawdowns are low, but in general are strongly non-linear and require numerical solution with a purpose written algorithm. Because these three situations are all solvable, and experimentally realisable, it is strongly recommended that a combined programme of experiment and modelling is conducted, so as to systematically compare model prediction and experimental observation in each case. This will allow the capabilities of the model to be assessed, and should indicate where the weaknesses are. Such a programme should also indicate what material properties need to be characterised, and how well, in order for the model to be used in predictive mode.

In simulations of sand pack depressurization (the so called PVT cell problems), both the linear mass transfer model, and the nucleation theory based model predict pressure versus time (or cell volume) curves that lie below those corresponding to equilibrium. Changing the relaxation time constant in the linear model changes the size of this offset (larger with longer relaxation times), and of course the rates of pressure and dissolved gas fraction adjustment. As mentioned above, only the nucleation theory based model predicts non-monotonic pressure versus time behaviour in a constant volume expansion rate test. It is not clear to me that the capability to predict this non-monotonic pressure behaviour is necessary for the mass transfer model to do a good job in reproducing pressure and volume fractions in a transient non-uniform core depressurization experiment. The minimal requirements on a mass transfer model, which no doubt depend on the uses to which it will be put, need to be determined. This is a topic for future work.

Simulations of steady flow through a core, using the nucleation theory based mass transfer model reveal that there is a flow rate threshold below which bubble nucleation occurs in a localised zone of small spatial extent, and above which nucleation occurs throughout the core. Furthermore, the average bubble size, at cessation of nucleation, decreases as the flow rate through the core increases. Thus, more and smaller bubbles are created at high flow rates than at low. These observations may have some implications for the search for explanations of the experimentally observed rate dependence of critical gas saturation; we might hypothesise that the dispersed phase gas saturation can reach higher values before large scale connectedness develops when the bubbles are small than when they are large. Experiments should be done to see if this predicted transition occurs in reality.

The observation of a flow rate threshold, separating localised from distributed bubble nucleation, is novel, and is very interesting because it is the first instance that I have been able to find in which solutions of the transport and transfer equations exhibit a transition in behaviour as some parameter is varied. If we believe that foamy production is qualitatively different from normal primary solution gas drive production, then, the model for foamy production must in some way differ from that for normal production. This difference may manifest itself only in the forms of constitutive terms, which are outside the capabilities of the present model itself to predict and must be externally input, or, as I imply here, may be heralded by the appearance of precursor phenomena or trends in solution properties within the solutions of the model. Decreasing bubble size and transition to non-localised nucleation may be precursor phenomena in this sense, although a firm logical argument that they must inevitably lead to a shift in the critical gas

saturation has not yet been made, and probably cannot be made without appeal to a pore scale model of gas-liquid distributions within the porous medium. This is a research topic for the future.

The nucleation model makes certain predictions about how bubble number and size vary with fluid and rock material properties. For example, the dependence of bubble size and number density on depressurization rate, on the diffusivity of dissolved gas within liquid, on surface tension, and on the number of potential nucleation sites may all, to some degree, be investigated within this model. This in turn may be indicative of what physico-chemical properties are important in determining whether a particular rock-fluid system will exhibit foamy production behaviour (by which we mean elevated total liquid recovery, or, a high value of critical gas saturation) or not. The steady core flow equations should be non-dimensionalized, and scaling parameter groups identified. A more complete study of how model predictions change as parameters are varied should be done. The implications for what physico-chemical properties of the rock-fluid system determine foamy versus non-foamy behaviour should be stated, and a programme of experiments to test these predictions made.

The preceding two paragraphs refer to a qualitative difference between foamy and normal primary production by solution gas drive, and yet, no definition of what is meant foamy primary production has been given ! Rather, it is defined by what it is not; total liquid recovery bigger than normal, produced gas less than normal, relative permeabilities abnormal [Maini]. The only generally agreed and positive element in Maini's categorisation is the statement that total liquid recovery increases with flow rate (the statement about the *flow* of gas in the form of small bubbles is not generally agreed; different experiments lead to different conclusions about gas bubble motion or trapping, and indeed the existence of very small gas bubbles is questioned by some authors [Pooladi-Darvish & Firoozabadi]). This situation is clearly not acceptable. We should aim to produce a definition of foamy behaviour which says what it is. The definition should be capable of being used to interpret a given set of experimental measurements to determine if the behaviour is foamy or not; that is, it should involve only quantities that are measurable (albeit with difficulty). Such a definition, together with an appropriate mechanistic model, should permit the planning of a programme of research towards identification of the crucial material properties of rock and fluid which determine foamy behaviour.

Lastly, two solutions for transient depressurization flow within a core are given, one using the linear mass transfer model, the other a simplified form of the nucleation theory based model. When the time constant in the linear mass transfer model is taken equal to zero, implying local equilibrium at all times between dissolved gas fraction and bubbles, the (non-linear) governing equations reduce to those familiar in conventional modelling of flow of a compressible fluid within a porous medium. Thus, any novel and specifically foamy phenomena must be associated with either with departures from composition equilibrium or with novel forms for, say, the dependences of the mobilities on dispersed gas volume fraction. A Laplace transform solution of the linear mass transfer problem, in circumstances where pressure disturbances are sufficiently weak that non-linear terms in the transport equations can be dropped, shows that a finite time scale for attainment of equilibrium changes the details of the solution for pressure disturbances, compared with the case in which equilibrium is instantaneously attained, over times comparable with the relaxation time scale, but does not significantly alter the overall character of the solution, which is essentially diffusive. Thus, finite relaxation times alone are not sufficient to introduce qualitatively novel behaviours, compared to conventional solution gas drive, into solutions for core depressurization flow, and if we seek these, we must introduce non-linearity, either in the mobilities or in the mass transfer process.

Non-linearity is introduced, to the mass transfer terms, when the nucleation theory based model is used. Because of the extreme complexity of this model, semi-analytical progress can only be made if significant simplifications are made, in particular, if the time scales for nucleation and non-equilibrium mass transfer are assumed short, and the nucleation and non-equilibrium growth processes are assumed to occur only in a narrow shock-like region across which a jump in gas bubble volume fraction occurs (so, the possibility of distributed nucleation at high flow rates is neglected). Unfortunately, even then, it is very difficult to calculate a solution, because, from the studies of steady flow in a core, it appears that the size of the bubble

volume fraction jump at the nucleation front depends on the speed at which that jump region moves into the core. This in turn means that a simple Stefan-type similarity solution (which is about the most complicated thing that can be dealt with by semi-analytical means) cannot exist. For these reasons, it is probably more profitable in the future to concentrate efforts on numerical solutions, and to use these to map out the behaviour of both the nucleation model and the non-linear (i.e. finite drawdown and volume fraction) form of the linear mass transfer model. In the investigations reported here the focus has been on the consequences of different assumptions about the mass transfer processes on the qualitative form of solutions. Variations in mobility with gas volume fraction also affect the character of solutions, and these must be studied too.

In order to get some insight into the structure of solutions of the nucleation model (which is useful for quality control of future numerical solutions), it was assumed that the volume fraction jump at nucleation is constant in size, and independent of the speed at which the nucleation zone advances. A Stefan type similarity solution then exists. Produced fluid flow rates decrease in time with an inverse square root of time scaling, and the larger the volume fraction jump at the nucleation front, or equivalently, the larger the supersaturation required to initiate nucleation, the smaller the produced fluid flow rate all other factors being held equal.

Bearing in mind these results, it is possible to speculate about the structure of solutions to transient core depressurization problems: When a finite supersaturation is required to initiate bubble nucleation and mass transfer, there is a propagating front, ahead of which the gas bubble volume fraction is zero, and behind which the bubble volume fraction is finite. The bubble volume fraction is larger at the core exit than at the nucleation front. Although not proven here, it seems likely that there are two classes of solution, one at low rates (or large times) in which nucleation occurs only in a small zone at the front, the other, at high rates or short times, in which bubble nucleation occurs everywhere behind the advancing front. When nucleation commences at essentially zero supersaturation, the front is so weak as to be effectively absent and the pressure and volume fraction move into the core following a non-linear diffusion-like process. Numerical solutions of the full non-linear problem must be made, to see if these speculations are valid.

A mathematical model for the flow within a permeable porous medium of an oil containing dissolved gas, and capable of liberating that gas as pressure falls to form bubbles or connected gas regions, has been presented, and its consequences worked out for a number of experimentally realisable situations. Some speculations have been made, based on the results of calculations made with the model, about the mechanisms that might underlie the observed differences between foamy and normal solution gas drive production behaviour. The question of whether this model is an adequate, or an excessive, description for the flow of a foaming heavy crude oil within a reservoir is still open, and can only be answered by a systematic programme of comparison of model predictions against experiment. This will require both that new calculations and new experiments be done.

This work was performed while the author was on a six month secondment to Intevep. He is grateful to the managements of Schlumberger and Intevep for making this opportunity possible, and to the members of the various heavy oil projects for information and encouragement. Special thanks are due to Arjan Kamp and Dan Joseph, whose thoughts have much influenced what is presented here.

References

[Abramowitz] M. Abramowitz & I. Stegun 'Table of Mathematical Functions' Dover (1975).

[Barclay et. al.] J. Barclay, D.S. Riley, R.S.J. Sparks 'Analytical models for bubble growth during decompression of high viscosity magma' Bulletin of Volcanology, **57**, 422-431 (1995).

[Blander & Katz] M. Blander & J.L. Katz 'Bubble nucleation in liquids' AIChE Journal **21**(5) 833 (1975).

[Firoozabadi & Kashchiev] A. Firoozabadi & D.Kashchiev 'Pressure and volume evolution during gas phase formation in solution gas drive process' SPE 26286 (1993).

[Firoozabadi, Ottesen & Mikklesen] 'Measurements of supersaturation and critical gas saturation' SPE Formation Evaluation 337-344 (December 1992).

[Hammond91] P.S. Hammond 'One- and two-phase flow during fluid sampling by a wireline tool' Transport in Porous Media, **6**(3), 299-330, (1991).

[Hammond97a] P.S. Hammond 'An extension of the Joseph model for formation flow of foamy heavy crude' memo dated 14 May 1997.

[Hammond97b] P.S. Hammond 'Some simple illustrative calculations with the extended Joseph FHC model' memo dated 26 May 1997.

[Hammond97c] P.S. Hammond 'FHC flow with continuous gas' memo dated 2 June 1997.

[Hammond97d] P.S. Hammond 'A FHC calculation illustrating the effects of finite bubble nucleation rates' memo dated 1 July 1997.

[Hammond97e] P.S. Hammond 'Foaming heavy crude model with independently flowing phases' memo dated 28 July 1997.

[de Hoog] de Hoog et. al. '… numerical inversion of Laplace transforms …' SIAM Journal of Scientific & Statistical Computing, **3**(3), 357-366 (1982).

[Huerta et.al.] M. Huerta, C. Otero, A. Rico, I. Jimenez, M. de Mirabal & G. Rojas 'Understanding foamy oil mechanisms for heavy oil reservoirs during primary production' SPE 36794 presented at Annual Technical Meeting, Denver, (1996).

[Joseph] D.D. Joseph 'Model of horizontal drilling hole in a reservoir of foamy oil' n.d. Intevep document.

[Li & Yortsos] X. Li & Y.C. Yortsos 'Theory of bubble growth in porous media by solute diffusion' Chemical Engineering Science **50**(5), 1247, (1995).

[Loughead & Saltuklarogulu] 'Lloydminster heavy oil production; why so unusual ?' paper presented at 9th Annual Heavy Oil and Oil Sands Technology Symposium, March 11, Calgary (1992).

[Lubetkin] S.D. Lubetkin 'Bubble nucleation and growth' in 'Controlled Particle, Droplet and Bubble Formation - (Colloid and Surface Engineering Series)' ed. D.J. Wedlock, Butterworth-Heinemann (1994).

[Maini] B.B. Maini 'Foamy oil flow in heavy oil production' Journal of Canadian Petroleum Technology **35**(6), 21, (1996).

[Maini & Sarma] B.B. Maini & H. Sarma, 'Role of non-polar foams in production of heavy oils' Advances in Chemistry series, **242**, 405-420, (1994).

[Pooladi-Darvish & Firoozabadi] M. Pooladi-Darvish & A. Firoozabadi 'Solution gas drive in heavy oil reservoirs' CIM paper 97-113 (1997).

[Satik, Li & Yortsos] C. Satik, X. Li & Y.C. Yortsos 'Scaling of single bubble growth in a porous medium' Physical Review E, **51**(4), 3286 (1995).

[Sheng et. al.] J.J. Sheng, R.E. Hayes, B.B. Maini & W.S. Tortike 'A dynamic model to simulate foamy oil flow in porous media' SPE 36750, presented at 1996 Annual Technical Conference, Denver, (1996).

[Smith] G.E. Smith 'Fluid flow and sand production in heavy oil reservoirs under solution gas drive' SPE 15094, presented at 56th California regional meeting of the SPE, Oakland, (April 1986).

[Toramaru89] A. Toramaru 'Vesiculation process and bubble size distributions in ascending magmas with constant velocities' Journal of Geophysical Research **94**(B12) 17523-17542 (1989).

[Toramaru95] A. Toramaru 'Numerical study of nucleation and growth of bubbles in viscous magmas' Journal of Geophysical Research **100**(B2) 1913-1931 (1995).

[Wilt] P.M. Wilt 'Nucleation rates and bubble stability in water-carbon dioxide solutions' Journal of Colloid and Interface Science **112**(2) 530 (1986).